EURAS JOURNAL of Engineering and Applied Sciences

EURAS JOURNAL OF ENGINEERING AND APPLIED SCIENCES

Volume 4 Issue 2 August 2024

Genel DOI: 10.17932/EJEAS.2021.024
Volume 4 Issue 2 DOI: 10.17932/EJEAS.2021.024/2024.402

EURAS JOURNAL OF ENGINEERING AND APPLIED SCIENCES

ISSN : 2757-7961

CONCESSIONAIRE on behalf of EURAS
Prof. Dr. Mustafa AYDIN

Editor in Chief
Prof. Dr. Hasan Alpay HEPERKAN
Department of Mechanical Engineering, Istanbul Aydin University, Istanbul, TURKEY
Mechanical Engineering Department Florya Yerleskesi, Inonu Caddesi, No.38, Kucukcekmece, Istanbul, Turkey
Fax: +90 212 425 57 59
Tel: +90 212 425 61 51 / 22001
E-mail: hasanheperkan@aydin.edu.tr

Associate Editor
Research Assist. Büşra Selenay ÖNAL
Department of Mechanical Engineering, Istanbul Aydin University, Istanbul, TURKEY
E-mail: bselenayonal@aydin.edu.tr

Administrative Coordinator
Sabina HUSEYNOVA

English Proofreading
Behcet Özgür ÇALIŞKAN

Graphic Design
Başak GÜNDÜZ

Language
English

Publication Period
Published issues per year: February, August

Volume 4 Issue 2 - August 2024
Correspondence Addres
EJEAS - EURAS JOURNAL OF ENGINEERING AND APPLIED SCIENCES
Adress: Beşyol Mah. İnönü Cad. No: 38 İstanbul - Türkiye
Phone: +90 (212) 411 61 68
E-mail: euras@euras-edu.org

Printed by
Levent Baskı Merkezi
Sertifika No: 35983
Emniyetevler Mahallesi Yeniçeri Sokak No:6/A
4.Levent / İstanbul, Türkiye
Tel: 0212 270 80 70
E-mail: info@leventbaskimerkezi.com

Editorial Board

Scientific Advisory Board

Contents

Research Article

DOI Numbers

General DOI: 10.17932/IAU.DENTAL.2015.009
Volume 4 Issue 2 DOI: 10.17932/IAU.DENTAL.2015.009/2024.402

Experimental Setup Design for Investigation of Flow Boiling Heat Transfer Characteristics of R-134a in Helically Coiled Tubes with Smooth and Corrugated Surfaces
Şafak KIRKAR
10.17932/EJEAS.2021.024/ejeas_v04i2001

Lack of Penetration of Welded Pipe and Stress Behavior
Tidjani AHMEDİ
10.17932/EJEAS.2021.024/ejeas_v04i2002

AI-Based Early Detection of Parkinson's Disease Using MRI: A Comparative Analysis of Densenet121 and Resnet Models
Ali Okatan
10.17932/EJEAS.2021.024/ejeas_v04i2003

Mechatronic System Design of Feeding Mechanism in Shuttlecock Launcher by Using Rotary to Linear Motion
Ali DORAGHİ
10.17932/EJEAS.2021.024/ejeas_v04i2004

Effect of Stacking Sequence on the Mechanical Performance of Hybrid Fiber Reinforced Epoxy-Polyester Composites
Fayçal MİLLİ
10.17932/EJEAS.2021.024/ejeas_v04i2005

From The Editor

Euras Journal of Engineering and Applied Sciences (EJEAS), is a peer-reviewed academic journal, establishing a solid platform for all academicians, consultants, researchers, and those who have a strong interest in global current issues and trends in engineering and applied sciences. Euras Journal of Engineering and Applied Sciences is based on engineering and applied sciences; artificial intelligence, cybersecurity, environmental sciences, food and food safety, biotechnology, material science and composites, nanotechnology, energy technologies, electronics, robotics, thermal sciences, earthquakes – structures – foundation and earth sciences studies. Subject areas could be as narrow as a specific phenomenon or device or as broad as a system.

EJEAS was established with the intention of promoting scholarly communication all over the world in a more effective manner. Our aim is to establish a publication that will be abstracted and indexed in the Engineering Index (EI) and Science Citation Index (SCI) in the near future. The journal has a short processing period to encourage young scientists.

Prof. Dr. Hasan HEPERKAN
Editor

Research Article

Experimental Setup Design for Investigation of Flow Boiling Heat Transfer Characteristics of R-134a in Helically Coiled Tubes with Smooth and Corrugated Surfaces

Safak Metin Kırkar[1], Ahmet Selım Dalkılıç[1]

[1,]Department of Mechanical Engineering, Faculty of Mechanical Engineering, Yildiz Technical University, Istanbul 34349, Turkey
**Corresponding author's e-mail address: smkirkar@yildiz.edu.tr*
Orcid id(s): 0000-0001-8800-8477, 0000-0002-5743-3937

ABSTRACT

Helically coiled tubes with two-phase flow are widely used instruments in numerous fields such as heating and cooling, energy production industry, chemical plants, etc. In academy and industry, optimum design considering the geometrical parameters and optimum working conditions of the heat exchangers are tried to find out in order to enhance the thermal performance, since the energy used is limited and valuable. In this study, an experimental setup for the investigation of flow boiling heat transfer characteristics in shell and helically coiled tube heat exchangers is presented and the procedure of the system is introduced. This paper can be considered as a guide for the researchers willing to design an experimental setup to investigate heat transfer characteristics of any fluids in helically coiled tubes or similar ones.

Keywords: *Experimental Setup, Flow Boiling, Heat Transfer Characteristics, Shell and Helically Coiled Tube Heat Exchangers*

1.INTRODUCTION

Heat exchanger is the device that transfers heat between the fluids. The rate of the heat transfer occurringbetween the fluids and pressure drops in the fluids determine the thermal performance of the heat exchangers. In order to produce more effective heat exchangers in terms of the thermal performance, some methods are used in the literature, namely active, passive and compound methods [1]. Passive heat transfer enhancement methods arepreferred more, since the external energy supplied is not required and relatively easier to establish [2]. Modifications on the tube surface such as corrugation, dimple, protrusion, rib and micro-fin, use of inserts such astwisted tape and wire coil, helically coiled tubes, use of nanofluids are common and well-known examples of thepassive techniques [3]. Surface enhancements on the tube increase the heat transfer surface area, provide flow to pass turbulence earlier, and cause swirl and vorticities at the secondary flow region, resulting in an increase in the heat transfer rate. The geometry of the helically coiled tube (i.e., its curvature) induces secondary flows to occur due to the centrifugal force, resulting in an enhancement in the heat transfer rate. Adding a certain amount of nanoparticles into the pure base fluid enhances the thermophysical properties of the fluid such as thermal conductivity, viscosity, and density, which in general causes the heat transfer rate to increase.

Some of the recent studies on flow boiling in helically coiled tubes available in the literature are summarized as follows. Kong et al. [4] experimentally performed subcooled boiling of R-134a in helically coiled tubes with vertical arrangement. The effect of heat flux, mass flux, inlet subcooled temperature and system pressure

on the heat transfer characteristics is researched. According to their main findings, there is no significant difference in the effect of operating conditions on the heat transfer characteristics between horizontal and vertical tube orientations. Heat transfer coefficient enhances with pressure but reduces with subcooling.

Niu et al. [5] studied flow boiling in helically coiled tubes with vertical orientation. An analytical modelis developed to estimate onset of dryout quality. They theoretically analyzed parameters such as heat flux, centrifugal force, density ratio, gravity, surface tension and interfacial shear force which influence the droplet entrainment and deposition characteristics having primary effects on the liquid film dryout. Also, the influence of coil

diameter, mass flux, heat flux, and system pressure on the onset of dryout quality and net entrainment rate is discussed. According to findings, onset of dryout quality diminishes with raise in mass flux, and net entrainment rate rises steadily with heat flux. In another study [6], they examined experimentally flow boiling of R-134a in vertically oriented helically coiled tube under high heat flux. The effect of thermal hydraulic parameters on the flow boiling heat transfer characteristics is presented. According to main findings, vapor quality enhances the heat transfer coefficient in low quality region under low heat flux condition, and it almost does not change in the case of high heat flux condition. Vapor quality smoothly increases the heat transfer coefficient in high quality region under high heat flux condition indicating convective boiling is weakened.

Hardik and Prabhu [7] experimentally investigated single-phase flow and flow boiling of R-123 in helically coiled tube. The influence of curvature of helical coil on two-phase pressure drop, local heat transfer coefficient and critical heat flux is studied. Heat transfer coefficient at the circumference of helically coiled tubepersists same with that of straight tube in the subcooled and nucleate flow boiling regions. Moreover, heat transfer coefficient at the outer side of the helically coiled tube is higher than that of straight tube in the convective flow boiling region. However, heat transfer coefficient at the inner side of the helically coiled tube is lower than that of straight tube. In another study [8], they analyzed experimentally flow boiling of R-123 and water in helically coiled tubes. The effect of geometrical parameters such as tube diameter and coil diameter, and operating parameters such as mass flux, heat flux, exit quality and density ratio on the critical heat flux is viewed. The collected data for critical heat flux is compared with the related correlations from the literature and a new correlation is suggested in the study.

Shah [9] conducted a comparison of data and correlations from the literature for saturated boiling heat transfer of water, refrigerants and helium in helically coiled tubes. Tube orientation, tube diameter, coil diameter, pressure and mass flux are the parameters taken into consideration. It is concluded that flow boiling heat transfer coefficient in helically coiled tubes can be estimated by reliable correlations for straight tubes, not for helically coiled tubes.

Prattipati et al. [10] numerically carried out subcooled flow boiling of water in helically coiled tubes. The influence of geometrical parameters such as

tube diameter and coil diameter, and operating parameters such as inlet subcooling, mass flux and wall superheat on the axial variation of void fraction. The void fraction in axial direction increases with coil diameter. On the other hand, liquid temperature rises with decreasing coil diameter. Mass flux and curvature ratio affects the phase distribution at the same quality, whereas inlet subcooling and wall superheat do not. Correlations for vapor quality, distribution parameter and drift velocity including the effect of the curvature are proposed for estimating void fraction variation.

From the studies, it is noticed that geometrical parameters such as tube diameter and coil diameter, and operating conditions of the working fluid such as pressure, mass flux, heat flux and vapor quality have significant effect on the flow boiling heat transfer characteristics of the fluid in the helically coiled tubes.From the literature, it is noticed that there are lots of studies reported on the heat transfer characteristics of single-phase and two-phase flows in helically coiled tubes, but a few studies on two-phase flows in enhanced surfaced ones. Single-phase flows in helically coiled tubes investigated highly including with enhanced surfaces and nanofluids. For two-phase flows, studies are mostly on helically coiled tubes with smooth surface and the working fluid used in the studies is water. It is observed that there is a gap in the literature on the investigation offlow boiling heat transfer characteristics of any fluids in helically coiled tubes with enhanced surfaces such as corrugated, micro-finned, dimpled.

2.SYSTEM DESCRIPTION

Figure 1.a shows the picture of the experimental setup and Figure 1.b shows the schematic of the experimental setup in which blue and orange lines correspond to the fluids of water and freon, respectively. The aim of such a setup is to investigate the two-phase flow heat transfer performance of helically coiled tubes with smooth and corrugated surfaces. In addition, the names of apparatuses mentioned with numbers in Figure 1.b are given in Table 1.

Firstly, liquid R-134a is pressurized with a pump to required pressure and to determine its volumetric flow rate, it flows through one of the rotameters which is suitable in terms of measurement range. Then, it passesthrough a plate heat exchanger in which liquid hot water conditioned in the hot water tank heats the freon until it becomes saturated liquid or liquid-vapor mixture with certain vapor quality. In this section, its inlet and outlet temperatures and pressures are measured with Pt100 type RTD sensors and

pressure transmitters, respectively. Also, the inlet and outlet temperatures of the liquid hot water are measured with Pt100 temperature sensors. And volumetric flow rate of the water is measured by a rotameter before it enters the plate heat exchanger. Here, vapor quality of the refrigerant can be determined precisely by energy balance equation derived for the plate heat exchanger. After it exits the plate heat exchanger, it enters the test section which is shell and helically coiled tube heat exchanger.

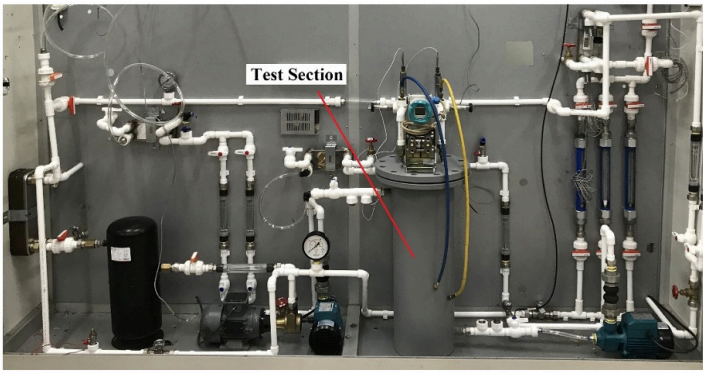

a)

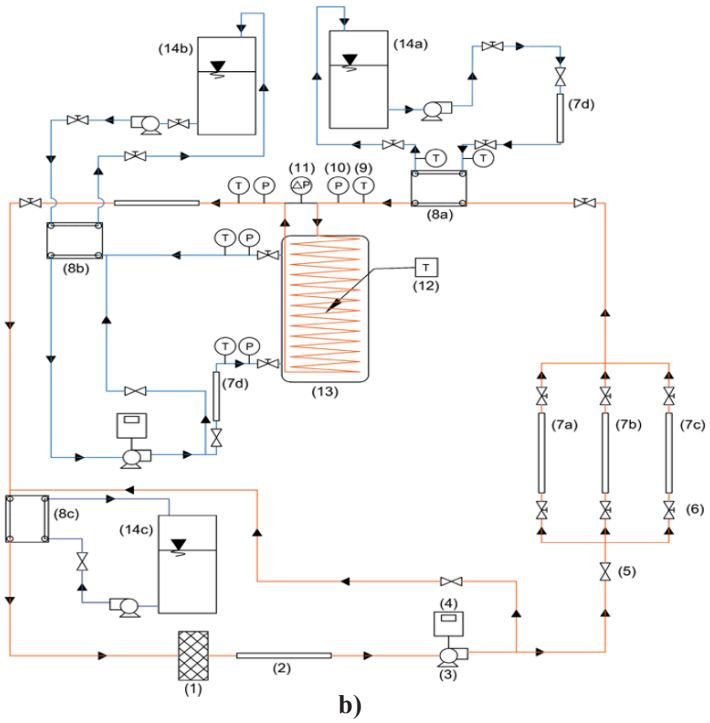

b)

Figure 1. a) Picture of the experimental setup and **b)** schematic of the experimental setup

Table 1. List of apparatuses used in the experimental setup

#	Apparatus	#	Apparatus
1	Liquid freon tank	8	Plate heat exchangers - a) evaporator, b) heater, c) condenser
2	Sight glass	9	RTD sensor
3	Circulating pump	10	Pressure transmitter
4	Frequency converter for pump	11	Differential pressure transmitter
5	Needle valve	12	Thermocouples at 10 equally spaced locations on the outer surface of the helically coiled tube
6	Ball valve	13	Test section: shell and helically coiledtube heat exchanger
7	Rotameters with different ranges ofmeasurement	14	Water conditioning tanks - a) hot, b)hot, c) cold

Here, R-134a flows in the tube side, while liquid hot water conditioned in another hot water tankflows through the annulus. As the heat transfer occurs between R-134a and liquid hot water, refrigerant evaporatesand water cools down. Since the refrigerant flows during this evaporation process, it is called as flow boiling. In the test section, inlet and outlet temperatures and pressures of the refrigerant and inlet and outlet temperatures of the liquid hot water are measured. Pressure difference between the inlet and the outlet of the tube is also measured with differential pressure transmitter. And the temperatures are measured at 10 equally spaced points on the outer surface of the helically coiled tube by T-type thermocouples in order to determine local and average surface temperatures and heat transfer coefficients. Volumetric flow rate of the water is also measured by a rotameter before it flows through the shell side of the heat exchanger. Just after R-134a leaves the test section, its phase is observed with a sight glass to ensure it is evaporated. Then, it enters another plate heat exchanger and here refrigerant is cooled by liquid cold water conditioned in cold water tank, and the phase of the refrigerant changes to liquid again. Eventually, the closed cycle is completed. It should be noted that all the measurements are taken for specific operating conditions when the system reaches its equilibrium regime to meet steady-state conditions. This experiment is repeated for different tubes and operating conditions to investigate the flow boiling heat transfer characteristics of R-134a in helically coiled tubes and to determine the effect of using corrugated surface on the thermal performance. With the collected experimental data, proper correlations for both flow boiling heat transfer coefficient and pressure drop in the helically coiled tubes with smooth and corrugated surfaces can be proposed.

Figure 2 shows the picture of the helically coiled tubes with smooth and corrugated surfaces used in the test section.

Figure 2. Picture of the helically coiled tubes with smooth and corrugated surfaces

The tubes are made of stainless steel 316. Each of the tube has the same length (L) of 18,160 mm. Helically coiled corrugated tubes have four-start inward corrugations in the helical form on its surface. Table 2 shows the geometrical sizes of the tubes.

Table 2. Geometrical sizes of the helically coiled tubes

#	Geometry	d_o [mm]	t [mm]	D [mm]	phc [mm]	N [-]	H [mm]	β [°]	pc [mm]	e [mm]	α [°]
1	HCT-S	9.52	0.6	150	11.52	37	426.24	1.4	-	-	-
2	HCT-C	9.52	0.6	150	11.52	37	426.24	1.4	24	3.5	51.25
3	HCT-S	12.7	0.6	150	14.7	37	543.9	1.787	-	-	-
4	HCT-C	12.7	0.6	150	14.7	37	543.9	1.787	24	3.5	58.97

In the literature, helix angle of the coil (β) is mostly defined as the acute angle between the helix of the coil and the line perpendicular to the axis of rotation of the coil, whereas helix angle of the corrugation (α) is the acute angle between the helix of corrugation and the axis of rotation of the corrugation. Inner diameter of the tube (d_i) equals to envelope diameter (d_n) for inward corrugation and equals to bore diameter (d_b) for outward corrugation. The difference between the envelope diameter and bore diameter equals to the depth of the corrugation (e).

3.CONCLUSIONS

In this study, sample of an experimental setup for investigating the flow boiling heat transfer characteristics of a refrigerant in shell and helically coiled tube heat exchangers is presented. R-134a evaporates during flowing in the tube side, while the single-phase liquid hot water cools during flowing in the shell side. Helically coiled tubes with smooth and corrugated surfaces are considered in the test section with identical geometrical tube and operating system parameters to observe the effect of enhancing the surface of the tube by corrugation on the thermal performance of the heat exchanger. The working procedure of the system is introduced, and the apparatuses used in the system is listed.

REFERENCES

[1] Dewan A, Mahanta P, Raju KS, Suresh Kumar P. Review of passive heat transfer augmentation techniques. Proc Inst Mech Eng Part A J Power Energy 2004. https://doi.org/10.1243/0957650042456953.

[2] Sheikholeslami M, Gorji-Bandpy M, Ganji DD. Review of heat transfer enhancement methods: Focus onpassive methods using swirl flow devices. Renew Sustain Energy Rev 2015. https://doi.org/10.1016/j.rser.2015.04.113.

[3] Liu S, Sakr M. A comprehensive review on passive heat transfer enhancements in pipe exchangers. RenewSustain Energy Rev 2013. https://doi.org/10.1016/j.rser.2012.11.021.

[4] Kong L, Han J, Chen C, Xing K, Lei G. An experimental study on subcooled flow boiling heat transfer characteristics of R134a in vertical helically coiled tubes. Exp Therm Fluid Sci 2017;82:231–9. https://doi.org/10.1016/J.EXPTHERMFLUSCI.2016.11.023.

[5] Niu X, Yuan H, Quan C, Zhao L. Dryout quality prediction for boiling two-phase flow in vertical helically coiled tubes. Appl Therm Eng 2018;128:982–92. https://doi.org/10.1016/J.APPLTHERMALENG.2017.09.034.

[6] Niu X, Yuan H, Quan C, Bai B, Zhao L. Flow Boiling Heat Transfer of R134a in a Vertical Helically Coiled Tube. Https://DoiOrg/101080/0145763220181470304 2018;40:1393–402.https://doi.org/10.1080/01457632.2018.1470304.

[7] Hardik BK, Prabhu S V. Boiling pressure drop, local heat transfer distribution and critical heat flux in helical coils with R123. Int J Therm Sci 2018;125:149–65. https://doi.org/10.1016/J.IJTHERMALSCI.2017.11.026.

[8] Hardik BK, Prabhu S V. Experimental correlation for critical heat flux in helical coils. Nucl Eng Des 2020;368:110759. https://doi.org/10.1016/J.NUCENGDES.2020.110759.

[9] Shah MM. Prediction of heat transfer during saturated boiling in helical coils. J Therm Sci Eng Appl 2019;11.

[10] https://doi.org/10.1115/1.4042354/369164. Prattipati R, Pendyala S, Prasad BVSSS. Void fraction in helical coils during flow boiling with inlet subcooling. Int J Heat Mass Transf 2021;168:120904. https://doi.org/10.1016/J.IJHEATMASSTRANSFER.2021.120904.

Research Article

Lack of Penetration of Welded Pipe and Stress Behavior

Tidjani Ahmed Zitouni[1*], Zohra Labed[2]

[1]Department of Mechanical Engineering Faculty of Sciences of Technology, University Frères Mentouri, Constantine, Algeria E-mail address: t idjani.zitouni@umc.edu.dz*

[2] Department of Mechanical Engineering Faculty of Sciences of Technology, University Frères Mentouri, Constantine, Algeria zohra.labed@yahoo.fr

0000-0003-3760-6279

ABSTRACT

Use of too low a welding current, the practical use of too slow a travel speed, and an incorrect torch angle, in common are the most effects can cause penetration defects In this methodological study, we will do some analyses of stresses concentration on welding throat area on Pipe manufactured by API 5l X52 material and carefully compare necessary results between a good welded pipe and another one lacked from penetration; for that we typically apply five different pressures to naturally limit the desired results, this numerical study reasonably requires using SOLIDWORKS for ultimate conception and launch simulation with ANSYS after importing the specific geometry.

Keywords: *Pipelines, welding, lack of material, welding throat*

1.INTRODUCTION

Pipelines realistically are the veins of modern cities and modern towns. They knowingly transport drinking water, gas, oil and much, much more for that, pipe welders are needed to wisely keep them working properly. They undoubtedly play a big role in the petroleum industry, working on the piping necessary for each step of the process of bringing gas to the pump: from the oil rigs that carefully extract the crude to the direct pipelines that transport it to the refineries that turn it into oil and gas [1].

Arc welding is taking two or more separate pieces of metal and joining them into one continuous or homogeneous section. We achieve coalescence, which means to blend or come together. In other words, the purpose of arc welding is to achieve fusion between the initially separate pieces of metal. The American Welding Society (AWS) defines fusion as "The melting together of filler metal and base metal (substrate), or of base metal only which results in coalescence" (ANSI/AWS A3.0 Standard Welding Terms and Definitions). Fusion occurs when you have atomic bonding of the metals.

The molecules of each separate piece of metal and the filler metal bond together when you have 1) atomic cleanliness and 2) atomic closeness (see Figure 2). This occurs with the arc welding such that the atoms of each piece of metal bond together with shared electrons to become one solid or homogeneous piece of metal [2].

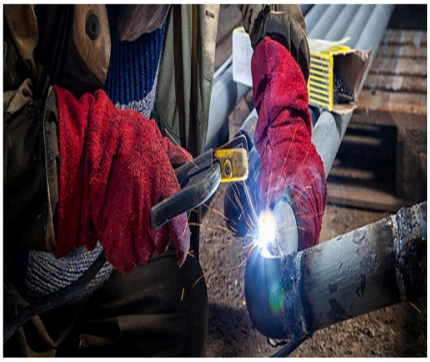

Figure 1. Pipe welding

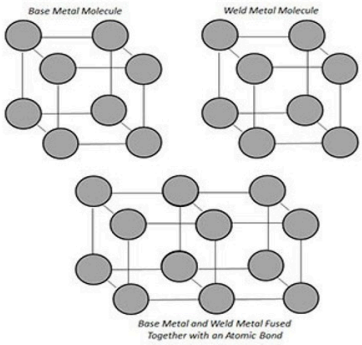

Figure 2. Atomic Bonding

2. CONCEPTIONS

Depending on the on Table 1 we design our geometry:Table 1:

Table 1. Dimension of Parts

Parts	Dout (mm)	Din (mm)	Th (mm)	Chamfer (°)
Pipe	63	54.40	8.6	30
weld joint	63+0.7	55	11	30

To create our defect, we will play on allowance of weld joint (Figure 3).

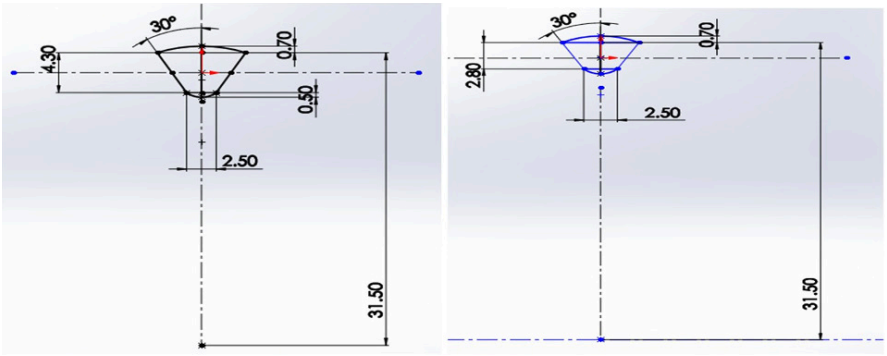

THE PERFECT WELDED JOINT **THE DEFECTED WELDED JOINT**

Figure 3. The two different joints used

The next figures show all parts in 3D (Figure 4, Figure 5) …

Figure 4. The pipe

Figure 5. The welding joint

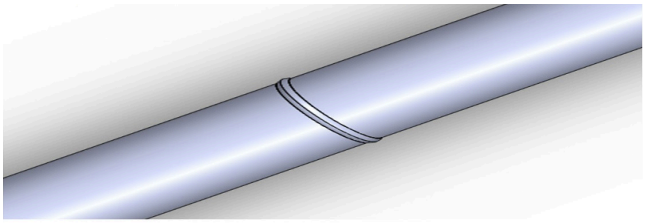

Figure 6. The welded pipe

After conception we and assemble parts (Figure 6) we define the two models of our study (Figure 7, 8).

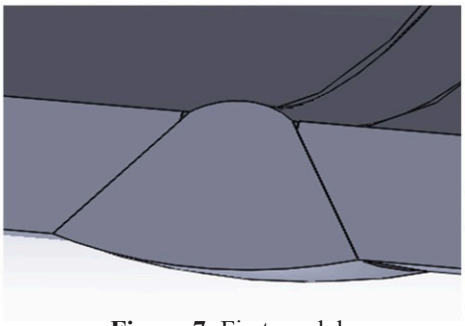

Figure 7. First model: Perfect welded joint

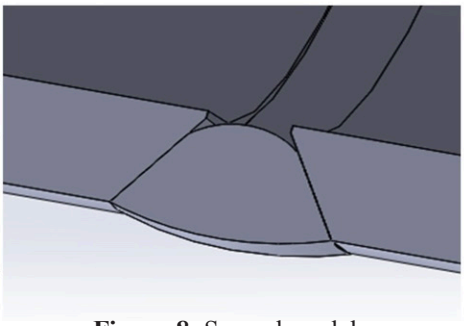

Figure 8. Second model: the defected welded joint

3.SIMULATIONS & RESULTS

For simulation we choose API 5L X52 Steel (look **Table 2**)

Table 2. Mechanical properties of the three zones

Zone	E (Mpa)	σYS (Mpa)	σUTS (Mpa)
BM	206.850	391.97	591.02
HAZ	206.850	363.01	616.20
WB	206.850	385.83	601.15

Here some Figures show Von Mises stresses for the two models after applying 50 MPa of pressure.

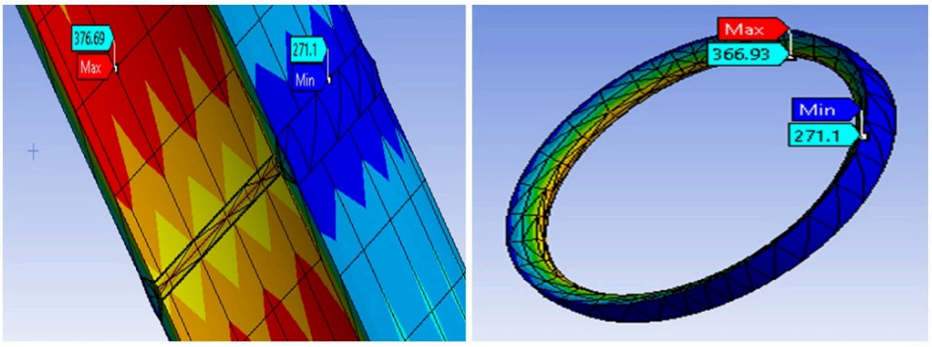

Figure 9. σ_{max} and σ_{min} model 1

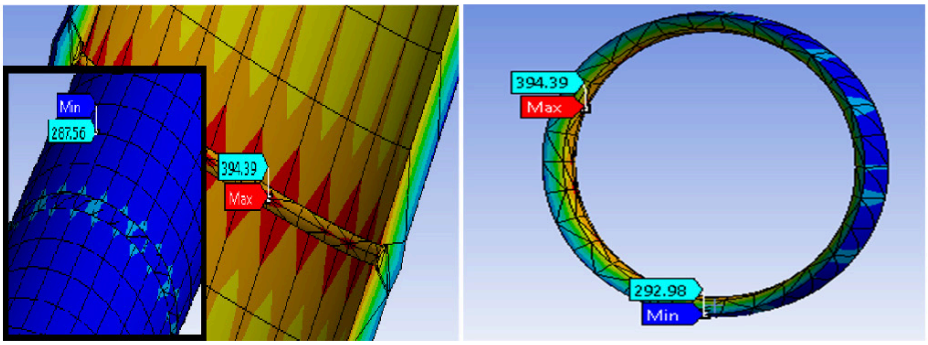

Figure 10. σmax and σmin model 2

Table 3. Stresses results with 5 different pressures for the first model

Applied Pressure (MPa)	Minimum Stresses (MPa)	Maximum Stresses (MPa)
10	54.22	75.337
20	108.44	150.67
30	162.66	226.01
40	216.88	301.35
50	271.1	376.69

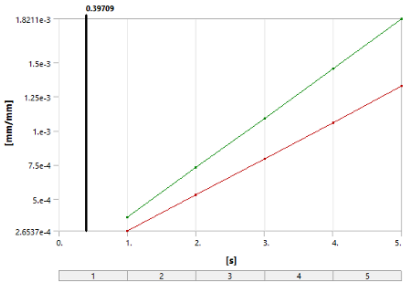

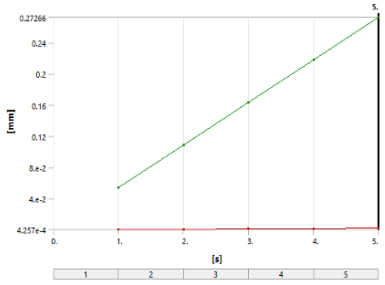

Figure 11. Equivalent elastic deformation **Figure 12.**Total displacement

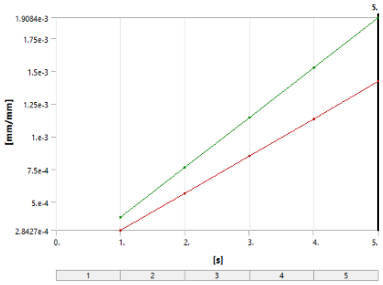

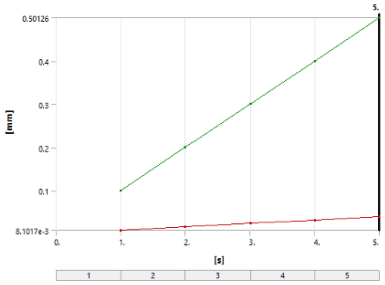

Figure 13. Equivalent elastic deformation **Figure 14.** Total displacement

4.CONCLUSION

From the previous results of tensile-strength test the first model shows that when we perform a good penetration the maximum stress point Stationed on the pipe that's mean the base metal and give 376.69 MPa, this value less than our maximum yield strength material, then this weld is accepted, without forget (Fig 13) and (Fig 14) tell that there is direct correlation relationship the first between the five applied pressure and deformation, the second between the pressures and displacement until 0.27 mm, but regarding second model with lack of penetration, thecritical zone stationed on weld joint that represent the weld bead we record in this area 394.39 MPa. When we compare, it's greater than the maximum yield strength for the three zones of API 5l X52 adding to all that increment in deformation and displacement. We conclude that we must have a good penetration in welding because its play a big deal in all geometries specially pipes. We mention the security side, for example defected weld create small's crack with time causes leakage or ruin of structure.

REFERENCES

[1] Zander Buel: What Is Pipe Welding, The Refrigeration school.Inc. (RSI) (2019).

[2] Support, Process and Theory: Weld Fusion vs. Weld Penetration, The Lincoln Electric Company (1999- 2019).

[3] Julio César Velázquez: On the Influence of the Corrosion Defect Size in the Welding Bead, Heat-Affected Zone, and Base Metal in Pipeline Failure Pressure Estimation: A Finite Element Analysis Study, Journal of Pressure Vessel Technology (2019).

[4] API Publishing Services, f 220 L Street, N. w., Washington, D.C. 20005: Welding of Pipelines and Related Facilities, American Petroleum Institute (1999). https://doi.org/10.1016/j.ijheatmasstransfer.2014.03.072.

AI-Based Early Detection of Parkinson's Disease using Mri: A Comparative Analysis of Densenet121 and Resnet Models

ALaa Im Abukaresh[2], Ali Okatan[1]

[1,2] Istanbul Aydin University, Istanbul, Turkey
[1]aliokatan@aydin.edu.tr, ORCID: 0000-0002-8893-9711
2alaaabukaresh@stu.aydin.edu.tr.

ABSTRACT

Parkinson's Disease (PD) is a neurodegenerative disorder that affects a significant portion of the population worldwide. Early and accurate diagnosis of PD is crucial for effective treatment and disease management. In this study, we propose an artificial intelligence (AI) model using deep learning techniques to detect PD at an early stage using Magnetic Resonance Imaging (MRI) data.The dataset used in this research is obtained from the Parkinson's Progression Markers Initiative (PPMI) and consists of 1,207 images, including 919 MRI scans from individuals diagnosed with PD and 288 MRI scans from healthy individuals. The dataset is pre-processed and augmented to enhance the robustness and generalization of the models. Two state-of-the-art transfer learning models, DenseNet121 and ResNet, are implemented and trained on the pre-processed dataset. These models are known for their ability to extract high-level features from medical images and have shown promising results in various image classification tasks. We leverage the pre-trained weights of these models, fine-tuning them on our specific PD dataset. Performance evaluation of the models is conducted using standard metrics such as accuracy and F1 score. Our results demonstrate that both DenseNet121 and ResNet achieve high accuracies, indicating their effectiveness in distinguishing between PD-affected and healthy individuals. DenseNet121 achieves an accuracy of 88.50% and an F1 score of 0.8847, while ResNet achieves an accuracy of 92.50% and an F1 score of 0.9247. The findings of this study indicate that AI models, particularly DenseNet121 and ResNet, have the potential to assist clinicians in the early detection of PD using MRI scans. The high accuracies achieved by these models demonstrate their ability to differentiate between PD-affected and healthy individuals based on imaging features. The utilization of transfer learning and pre-trained models reduces the need for large amounts of labeled data and enhances

the generalization capabilities of the models. In conclusion, this research contributes to the field of medical imaging and AI by presenting an effective approach for the early detection of PD using MRI data. The proposed DenseNet121 and ResNet models offer promising results and demonstrate the potential of AI in assisting healthcare professionals in accurate PD diagnosis. Further research and validation on larger and diverse datasets can help enhance the reliability and generalization of the proposed models for real-world clinical applications.

***Keywords**: Parkinson's Disease, binary classification, Convolutional Neural Networks, Transfer Learning, DenseNet121, ResNet, MONAI.*

1. INTRODUCTION

A vital component of human life has always been and will continue to be healthcare. Because of the dreadful and rapid advancement of technology, which affected every part of life, both scientists and medical professionals were keenly interested in how to diagnose diseases. In addition to helping with disease diagnosis, technology has also been used to perform surgeries and calculate medication dosages. Biomedical imaging technologies like Magnetic Resonance Imaging, computed tomography, X-rays, and positron emission tomography are used for diseases diagnose. As a result of the increased use of technology nowadays, The management of expanding imaging data is becoming a problem for healthcare providers. [35] High-performance computational tools, on other hand, accelerate the analysis of biomedical imaging data while reducing the radiologist's burden. Additionally, this technical advancement has made it possible for researchers to work with data and clinical models that are more complicated.[4] The term "neurodegenerative disease" (ND) is widely used to characterize cognitive impairments that impede a person's ability to think, walk, communicate, and learn. ND refers to issues with the brain. Some neurological diseases severely affect brain cells, creating unrelenting suffering that could potentially put a person's life in peril. Therefore, reducing the death rate depends on increasing public knowledge of this ailment. and the most prevalent NDs which are typically identified in older persons are Parkinson's disease and Alzheimer disease.[5] Parkinson's disease is a neurological ailment that progresses over time and is defined by several motor and non-motor symptoms which significantly lower life quality. The movement disorder falls under the extrapyramidal disorder category and has no known cause. There are various extrapyramidal illnesses

with other causes, such as vascular dementia, injury, sopori c-generate, carbon monoxide toxin, etc. that are categorized as Parkinsonism. Four main symptoms of the disease—tremors, rigidity, bradykinesia, and postural instability—are caused by the dopaminergic neurons loss in the substantia nigra and basal ganglia. Depending on how severe the symptoms are, Parkinson's disease is divided into mild, moderate, and advanced categories. Although idiopathic Parkinson's disease affects most patients, 20% are thought to be inherited. Genetic characteristics may distinguish Parkinson's disease subtypes, but more research is required before genetic information can be included in data-driven algorithms. Parkinson's disease has no known cure, however, the symptoms can be controlled with medicines and surgery. The Hoehn and Yahr (HY) scale and the Uni ed Parkinson's Disease Rating Scale (UPDRS) are two scales used to measure disability and impairment in Parkinson's disease. Parkinson's disease is the most common neurological disorder after Alzheimer's disease. Although the prevalence of Parkinson's disease rises with age, only 4% of patients have the situation when they turn 50. Parkinson's disease is more common in men than in women.[39] Parkinson's disease is thought to afflict 7 to 10 million people worldwide. The risk of acquiring Parkinson's disease may be increased by excessive exposure to chemicals like pesticides and herbicides.

Computer vision enables machines to think and understand more like people do. Computer vision is a catch-all phrase for all calculations using visual content, such as pixels in photos, videos, and other media. Numerous vision applications for computer vision exist, including computer-aided diagnosis in medicine, autonomous vehicles, and robots that can move and see like people. With the aid of extremely complex vision functions, computers may now act much like a human eye thanks to computer vision technology. With eyes that can collect light, brain receptors that can access it, and a visual cortex that can comprehend it, humans have extraordinary visual abilities. 30 years ago, significant strides have been implemented toward transferring great human visual abilities to machines. These algorithms for vision applications use deep learning and machine learning to analyze visual information similarly to how the human brain does. Applications for computer vision are in greater demand than ever. There are several repetitive operations in every area, including finance, healthcare, and marketing, that may be quickly automated utilizing computer vision techniques.

Neuroimaging is the most popular technique and prerequisite for the proper diagnosis and treatment of disorders that impact the neurological system. To differentiate between common variations, aging-related alterations, and acute/persistent illnesses, is crucial. As a result, the brain anatomy can be understood and visualized along with the brain tissues. This makes it easier to visualize and comprehend the structural changes in the brain by building representations of the brain from various perspectives.

The investigation of disease heavily relies on the location of anomalies seen on images. The neuro-radiologist then begins studying after identifying the anomalies and merges the imaging results and clinical data, which results in a thorough diagnosis.

Medical imaging has made incredible strides, but there are still many obstacles to overcome because of access restrictions and quality variances. So artificial intelligence and machine learning have become potent tools in recent years, offering algorithms that can resolve categorization issues in neuroimaging data.

One of the most important goals of neuroimaging techniques produce images of inside body structures to visualise and comprehend the anatomy of internal brain systems without surgery for better examining and diagnosing brain illnesses. There are numerous methods for taking pictures of the brain. The following imaging techniques are used: positron emission tomography (PET), functional magnetic resonance imaging (F-MRI), structural magnetic resonance imaging (S-MRI), resting state magnetic resonance imaging (rs-MRI), and single-photon emission computed tomography scan (SPECT).

These neuro-imaging techniques can produce high-dimensional images of the brain in axial, sagittal, and coronal views. For better diagnosis and therapy, doctors can distinguish between a healthy brain and a damaged brain using the varied ways that these other planes visualise brain structure. The field of radiology is being revolutionized by the emergence of artificial intelligence (AI), which aims to simplify the process of medical image interpretation. By utilizing computer vision, in which AI systems are capable of automating tasks such as measurements, identifying abnormalities, and analysing relevant anatomical structures. This transformation technology converts clinical input data into readily interpretable information, facilitating more efficient and accurate radiological diagnoses.[1]

ResNet, AlexNet, LeNet, VGGNet, MobileNet, DenseNet, and GoogLeNet are a few examples of popular CNN-based architectures designed to improve image categorization performance.

Neural Networks, Decision Tree ,Random Forests, Naive Bayes, and Support Vector Machines are other computer vision techniques used in picture classification. In contrast to deep learning techniques, machine learning techniques require intentional feature engineering.

Transfer learning models and neural networks offer the advantage of eliminating the manual feature extraction process. This automation allows deep learning models to fully automate multi-class or binary classification tasks. Even so, when it comes to handling large datasets, these traditional neural networks may encounter certain limitations that can impact their performance, particularly in computer vision tasks.

Diagnosing Parkinson's disease (PD) poses significant challenges because of the reliance on subjective symptoms and clinometric tests, which lack definitive confirmation. Also, Manual assessment methods are time-consuming, resource-intensive, and require expertise, leading to inconvenience and high patient costs. There are many techniques used to diagnose Parkinson's Disease such as Finger Tapping Tests and handwritten drawings that can identify upper limb impairments but these techniques cannot confirm PD diagnosis. Additionally, PET scans can only detect PD after significant dopamine neuron loss, hindering early intervention. SPECT images, while capable of examining dopamine activity, are limited in their ability to see structural changes, resulting in many false diagnoses. The invasive nature of generating PET or SPECT images with radioactive tracers further restricts their clinical use. Moreover, SWI, which detects PD through brain iron decomposition, is limited by anatomical structures. Furthermore, the availability of smaller datasets for PD diagnosis hampers accuracy assessment and increases the risk of over-fitting in diagnostic techniques.

Given the rising prevalence of PD and its effects on patients ' lives, it is needed to create a decision-support system to handle these issues. Computational tools, such as Artificial Intelligence techniques, have the potential to assist clinicians deciding accurate decisions regarding PD. Remote patient monitoring through web access and advanced telecommunication systems can reduce the inconvenience and cost of

physical visits. Still, reliable clinical monitoring tools are necessary to utilize these opportunities effectively. Speech problems, including slurring and weak voice, are common in PD patients, emphasizing the importance of accurate classification and early prediction. Currently, clinical diagnoses rely on subjective assessments and neurological testing, such as the Unified Parkinson's Disease Rating Scale (UPDRS), which may not be effective in the early stages of PD. Therefore, the development of automated Artificial Intelligence-based methods is essential to improve the accuracy of PD diagnosis and support better decision-making for clinicians.

2. LITERATURE REVIEW

Nowadays, computer-assisted prognosis is more prevalent in the healthcare industry. Even though the diagnosis approach for Parkinson's disease requires taking into account neurological examination and, clinical records, however, there are several studies based on Magnetic Resonance Imaging which is used to diagnose the disease in many literature.

A survey and overview of computer vision methods used to examine neuro-images for neurodegenerative illnesses are provided in specific papers. They discuss how computer vision techniques are used in neuroimaging analysis and how this could affect how neurodegenerative diseases are identified and understood, like the survey proposed by the authors Khan and Kaushik [(1)]: a comprehensive survey of computer vision techniques used to analyze neuro-images of patients suffering from neurodegenerative diseases. They discuss the growing prevalence of these diseases and the need for early diagnosis and review various computer vision techniques, such as image segmentation, registration, classification, and clustering, that are commonly used in neuro-image analysis. They also highlight the challenges associated with neuro-image analysis and how computer vision techniques can help overcome them. The paper provides a detailed review of various studies and research works in the field of neuro-image analysis using computer vision techniques and emphasizes the potential of computer vision techniques in improving the accuracy and efficiency of neuro-image analysis for neurodegenerative diseases.

Additionally, Khan, Yusera Farooq, and Baijnath Kaushik[(14)] discuss using computer vision algorithms in the analysis of high-resolution medical pictures, particularly neuro-imaging data obtained from modalities like MRI, CT, PET, and SPECT. The focus is on detecting, predicting, and diagnosing neurodegenerative diseases such as Alzheimer’s and

Parkinson's, which involve the progressive deterioration of neuronal cells in the human brain. The article highlights the computer vision techniques and its rols, such as image classification and identification, in interpreting neuroimaging data. The authors also discuss successful CNN-based architectures such as ResNet, AlexNet, LeNet, VGGNet ,and GoogLeNet which enhance image classification performance. In conclusion, computer vision is emerging as a critical tool to process medical images, enabling more efficient detection, prediction, and diagnosis of neurodegenerative diseases.

On the other hand, some articles have been devoted to the categorization of Parkinson's Disease (PD) utilizing MRI data employing deep learning methods, especially Convolutional Neural Networks (CNNs). They emphasise the promise of deep learning in enhancing diagnosis accuracy as they analyze various architectures, approaches, and performance indicators for PD classification. Explores the application of deep learning techniques, particularly Convolutional Neural Networks (CNN), in the categorization of neural brain images to distinguish or identify brains with Parkinson's disease (PD) from healthy brains. The dataset utilized in the study included 24 elderly ordinary control people aged 60 to 75 years old and 30 patients with PD with no history of neurological or medical disorders. As part of the pre-processing steps for the anatomical data, the Brain Extraction Tool was utilised to remove non-brain tissue from T1 anatomical images. After that, the images were converted into a stack of 2D PNG images. In the basic model, the author used three layers of the 2D convolution layer, each with a 'ReLu' activation function, followed by 2-3 max-pooling layers, a flattened layer, and two dense or fully connected layers, with final layer having two neurons corresponding to each of the two output classes (PD or normal). Without batch normalisation, the model's accuracy was 97.63%; with batch normalisation, it was 97.91%. The authors contend that more complex systems or other medical image categorization applications can be successfully implemented using the same architecture.[(2)]

Also, Dr. Naif Alsharabi and his team[(5)] proposed a hybrid model that integrates classical transfer learning and quantum transfer learning to diagnose neurodegenerative diseases using MRI data. The model extracts informative features using a pre-trained AlexNet model and then feeds this network into a quantum variational circuit (QVC) to transform the data into a 2-dimensional vector for binary classification of brain disorders. The

AlexNet-quantum learning model achieved high accuracy in classifying Alzheimer's disease and Parkinson's disease when compared with a classical transfer learning model. The proposed method could provide viable solutions in healthcare, with potential future applications in real quantum hardware devices and multi-classification tasks in computer vision.

Developing a 3D convolutional neural network to achieve early diagnose of Parkinson's Disease using 3T T1-weighted MRI scans from the Parkinson's Progression Markers Initiative database was the goal of Sabyasachi Chakraborty [(6)] .The study found that the created 3D CNN model successed with 95.29% as an overall accuracy, 0.943 as an average recall, average precision of 0.927, and 0.936 for f1-score of every class. This model placed the most emphasis on substantia nigra region of the brain for determining if a given MRI image indicated as Parkinson's Disease. The study concludes that results are encouraging; additionally, researchers need to enhance the detection of Parkinson's Disease using more efficient architectures and specific subcortical structures.

Even though Nikhil J. Dhinagar and his team[(7)] proposed a deep learning approach for the Parkinson's disease (PD) and Alzheimer's disease (AD) classification depending on 3D T1-weighted brain MRI. The authors used many datasets for training a 3D convolutional neural network (CNN) model, including the Parkinson's Progression Markers Initiative (PPMI), the Alzheimer's Disease Neuroimaging Initiative (ADNI), and the Open Access Series of Imaging Studies (OASIS) dataset. They also applied a random forest classifier as a basic model. For both PD and AD classification tests, the 3D CNN beat the random forest classifier, for PD classification using PPMI test set, the ROC-AUC was 0.667 and for UPenn dataset, they obtained ROC-AUC of 0.743. On the other hand, and for AD classification, when the ADNI test set was used, the ROC-AUC was 0.878, even though using OASIS dataset the average ROC-AUC was 0.789. For unseen MRI data from several data centres, the suggested model also generalised well. The authors suggest that this model could be a useful screening tool before more invasive procedures like PET scans and CSF assays and help distinguish between problematic cases of PD and AD whether their motor and non-motor symptoms are similarly mild.

To identify Parkinson's illness using MRI slices, Erdaş, Ç.B., Sümer, E [(8)] introduce a supervised deep learning technique. The suggested method

uses 3D T1-weighted MR images with median slices in the axial, coronal, and sagittal planes to detect neurodegeneration in the brain. The technique combines an AlexNet architecture and a CNN deep learning model to identify images in this new format. Classification performance of 90.36% accuracy and 90.51% area under the ROC measure was achieved using the suggested strategies. According to the study's conclusions, the suggested method can detect brain degradation on median slices of MR images, is a useful technique to diagnose Parkinson's disease. To strengthen the classifier's stability in future studies, the authors emphasize that new datasets should be added to the block of datasets that are already there.

Sajeeb, Asaduzzaman[11] proposes a prediction model for detecting Parkinson's disease (PD) due to deep learning techniques using neuro-images. To accurately classify PD patients, the model utilizes convolutional neural network (CNN) architectures, including VGG19, ResNet50, and InceptionV3. The study found that VGG19 had the highest accuracy among the three models tested. Further improvement can be made by including more complicated network topologies and convolutional layers in upcoming research, enabling doctors to detect PD more precisely and effectively.

Veetil, Iswarya Kannoth[13] evaluates the performance of five deep learning architectures for refining the diagnosis of Parkinson's disease using MRI images. Due to the growing accessibility of public information, sophisticated machine-learning algorithms have been created to aid in the classification and preliminary risk assessment of PD's patients. This study evaluates and contrasts the performance of five deep learning architectures, including VGG16, VGG19, Xception, ResNet50, and DenseNet201, using a variety of performance metrics, including classification accuracy, F1 scores, number of training epochs, model complexity, and depth of the network model. Transfer learning is used as the primary analytical technique. Three of the five models taken into consideration perform noticeably better than the existing work utilising the AlexNet model, according to testing of the models without hyperparameter adjustment. This research demonstrates the possibility of artificial intelligence as a decision assistance system for MRI-based Parkinson's disease diagnosis.

In Paper [15], Kumaran, R., and S. Shanthini present a hospital application that uses a modified VGG Net architecture to accurately detect Parkinson's disease from MRI scans without needing multiple consultations from

different doctors. The project aims to decrease the time and rate of human error associated with manual interpretation of medical images. The methodology involves improving the dataset, which involves MR scans, obtaining a trained model applying the VGG-16 architecture, and efficiently performing classification for patients using different CNN models. The ResNet-50 architecture is the most optimal. A web application with JavaScript framework reactJS is published as a front-end interface for the project. The paper concludes that the project helps cost-effectively provide efficient treatment and prevents the rate of human error associated with manual classification.

In the context of using Deep Learning for Neurodegenerative Disease Diagnosis using Neuro-Images, some papers propose deep learning approaches for the diagnosis of neurodegenerative diseases, such as Alzheimer's Disease (AD) and Parkinson's Disease (PD), using neuro-images. They utilize specific deep learning architectures and explore the potential of graph theoretical metrics and machine learning techniques in diagnosing and prognosis these diseases. Examples of these researchers were:

Kazeminejad, Amirali, Soroosh Golbabaei, and Hamid Soltanian-Zadeh[10] explored the use of graph theoretical analysis and machine learning techniques for the diagnosis of Parkinson's disease (PD) using resting-state functional magnetic resonance imaging (rs-fMRI) data. 19 PD patients and 18 healthy controls are included in the study, and the data undergoes several preprocessing steps before constructing a brain network graph using 90 regions of interest and their average time series. Global graph theoretical metrics are then extracted, including characteristic path length, efficiency, clustering coefficient, transitivity, and small-worldness, to investigate the ways in which PD patients' brain connection is altered. The study finds statistically significant increases in characteristic path length and decreases in segregation metrics and efficiency in PD patients. These alterations are not limited to a specific threshold, indicating aberrant functional connectivity at a larger scale. The study also uses local metrics, including centrality and nodal degree, as features to train a support vector machine classifier. The classifier can achieve a diagnostic accuracy of 95% when subjected to a leave-one-out cross-validation test. The five best features selected by the floating forward automatic feature selection method related to the cuneus (right hemisphere), precuneus (left), superior

(right), and middle (both) frontal gyri, which have all been noted to change in Parkinson's disease previously. Overall, the study confirms that Parkinson's patients' symptoms are correlated with broad changes in their brain networks. and shows the potential of employing machine learning and graph theoretical metrics for identifying diseases.. The findings suggest that PD symptoms are related to dysfunctional networks and the aberrant communication between these networks.

And Qiu, Anqi[12] developed a deep learning model, called graph-CNN-RNN, for the prognosis of Alzheimer's disease (AD) using brain structural MRI scans. The model was tested against the Open Access Series of Imaging Studies-3 and the other half of the Alzheimer's Disease Neuroimaging Initiative dataset. With an accuracy of about 80%, the graph-CNN-RNN predicted the conversion to AD from 0 to 4 years before the onset of AD. The positron emission tomography-measured amyloid load and clinical characteristics were both related to the AD probability risk. According to the study, there is a lot of opportunity for clinical applications of the graph-CNN-RNN and the AD probabilistic risk in the prognosis of AD. The model predicts the diagnosis of controls, moderate cognitive impairment, or Alzheimer's disease at each time point and lowers the dimensionality of the cortical thickness data.

Albu, Adriana[9] presents a binary classification algorithm to predicte the presence of malignant lesions in prostate cancer using three-dimensional magnetic resonance imaging (MRI) and convolutional neural networks (CNNs). The paper highlights the need for faster and more accurate diagnosis of prostate cancer, as traditional methods such as biopsies and histopathologic tests are time-consuming and depend on the radiologist's experience. The proposed algorithm reduces the time taken for investigations and could be a starting point in the diagnosis phase. The authors evaluated several models and chose the most performant architecture using the PyTorch and MONAI frameworks, which provide the following:

- Technical support.
- Optimization in training and evaluation phases.
- Compatibility with multiple operating systems.

The following steps for this research involve integrating the model into an application with a graphical user interface and developing algorithms to detect and segment the lesions to improve the application's accuracy.

Sabyasachi Chakraborty and the research team[23]: aimed to look into the early diagnosis of Parkinson's disease, a neurodegenerative condition brought on by the loss of dopaminergic neurons. The PPMI database of 406 people, half healthy and half of whom had Parkinson's disease, provided the 3T T1-weighted MRI images used in this investigation. The data was pre-processed, and a 3D convolutional neural network (CNN) was developed to learn patterns in the MRI scans for detecting Parkinson's Disease. The 3D CNN developed network performed great average outcomes, with an accuracy of 95.29%, a recall of 0.943, 0.927 precision, 0.943 for specificity, f1-sc0re was 0.936 and ROC-AUC score of 0.98 for both classes. The study shows the possibility of 3D CNNs for early Parkinson's disease detection, which can enhance patient outcomes and lessen the financial burden on governments.

Raj, Sini S., et al.,[16], proposed a deep learning-based automated segmentation algorithm to quantify iron accumulation in the deep gray matter structures of the brain in degenerative Parkinsonian disorders. Pathological iron deposition is evident in the degenerating brain areas of neurodegenerative disorders such Parkinson's disease, Multiple System Atrophy, and Progressive Supranuclear Palsy, which induce irregularities in bodily movements and posture.The Quantitative Susceptibility Mapping technique can quantify iron deposition, however, manual annotation of areas of interest (ROIs) takes time and may be accompanied by inter-rater differences.The proposed model uses a pre-trained deep learning model called Segnet for pixel-label-based semantic segmentation to automatically segment deep gray matter structures from MRI images, allowing for easy calculation of the amount of iron deposition. This method can effectively aid in precisely quantifying iron deposition, a crucial determining factor in developing Parkinsonian disease in the elderly community. However, the article highlights that While there are numerous ways to make learning on smaller datasets easier, the remarkable achievements of deep learning still require highly annotated large medical datasets.

Using Transfer learning techniques with Deep neural Networks to detect Parkinson's disease. Using fMRI data, Sakib, A. F. M., Sanjida Ali Shusmita, and S. M. Kabir[17] aimed to detect Parkinson's Disease and distinguish between those with the condition and the control group. They used the integration of Deep Neural Networks and Transfer Learning to develop three models - InceptionV3, VGG16, and VGG19. The models accuracy is compared and evaluated, and the dataset for this research is collected from

the Parkinson's Progression Markers Initiative (PPMI) repository. The results indicate that VGG19 gives the best accuracy at 91.5%, followed by InceptionV3 at 89.5% and VGG16 at 88.5%. The input data were amassed from the PPMI database, and MRI images were acquired in slices, which were then processed into the CNN models to extract features from the data group. The prediction model is obtained, and the subjects are tested to determine whether they have PD or are in the control stage.

Anupama Bhan[21] focuses on the early diagnosis of Parkinson's disease using brain MRI data and employs a deep learning algorithm for detection. This paper describes using a deep learning algorithm the detection of Parkinson's disease in brain MRI images. MRI can capture changes in the brain structure due to dopamine deficiency. Early diagnosis is crucial for effective treatment, and computer-aided diagnosis can assist clinicians in achieving this objective. The study uses a Convolutional Neural Network (CNN) with the LeNet-5 architecture to classify MRI data of Parkinson's disease subjects from normal controls. Dataset contained 10,548 images, and the model achieved 97.92% as an accuracy with batch normalization and dropout algorithms. The study concludes that this method can be used for diagnosing different stages of Parkinson's disease, and the model's accuracy can be further optimized by changing the number of neurons, kernel size, and layers and using the dropout algorithm. This research has the potential to facilitate feature extraction, selection, and classification for the prediction of new data in medical and neuroimage analysis.

On the field of Classification of PD using Machine Learning and Medical Imaging , there have been many studies, most notably were in (18) (20) (24) (25) (27) (29):

A Bayesian Optimisation Support Vector Machine (BO-SVM) model is presented by Elshewey, Ahmed M., et al.[18] for identifying Parkinson's disease (PD) patients and non-patients. SVM, Random Forest, Logistic Regression, Naive Bayes, Ridge Classifier, and Decision Tree are six machine learning models that the proposed approach uses Bayesian Optimisation to optimize the hyperparameters. 23 features and 195 cases make up the dataset used in this study. The trial findings showed that the SVM model generated the best results with an accuracy of 92.3% after hyperparameter modification using BO. The potential of using BO to improve the accuracy of machine learning models for categorizing PD is highlighted by this work.

Çağatay Berke Erdaş and Emre Sümer [20] propose a supervised deep-learning method to detect neurodegeneration in the brain, particularly the substantia nigra, using median slices from 3D T1-weighted MR images. This method achieved 90.36% as an accuracy, an area under the ROC curve of 90.51%, a precision of 90.08%, a sensitivity of 90.52%, and 90.25% for F1 score for the classification of Parkinson's disease patients from a control group of healthy individuals. The promising results indicate that computer-aided diagnosis based on medical images can be effective for Parkinson's disease detection. However, they pointed out certain drawbacks, such as the loss of proportion in resized sliced slices and the classifier's dangerous operation due to insufficient Neurocon and Taowu MRI Data Set samples. Adding more datasets is required to enhance the performance of the approach.

Roshni Saha[24], working on her thesis "Classification of Parkinson's Disease Using MRI Data and Deep Learning Convolution Neural Networks," discusses the use of deep learning algorithms, specifically Convolution Neural Networks (CNNs), for the classification of neural brain images to identify Parkinson's Disease affected brains from normal healthy brains. The accuracy reported by the author for separating MRI data from PD patients from normal controls was 97.63% without batch normalisation and 97.91% with batch normalisation. The study contends that CNN can efficiently classify additional medical images or more sophisticated systems and has the capacity to extract the most discriminative elements from complex clinical data. The method, according to the author, can also be used to forecast different Parkinson's disease stages for people of different ages and to research dementia and cognitive decline associated with Parkinson's disease.

Focusing on Parkinson's disease classification using convolutional neural networks applied to SPECT imaging data. Jigna Hathaliya[25] a classification model for Parkinson's disease using single-photon emission computerized tomography (SPECT) imaging data and a convolutional neural network (CNN). Based on the amount of dopamine in the brain, the model hopes to categorise patients and reduce the resources consumed while maintaining the model's performance. Data amplification was used to balance the unbalanced dataset and was preprocessed from the Parkinson's Progressive Markers Initiative (PPMI) dataset. Input layers, convolutional layers, max-pool layers, flattened layers, and dense layers with various dimensionalities are among the 14 layers in the proposed model. The dense layer divides

the patients into four groups: GenReg PSD from the full SPECT imaging dataset, PSD, healthy controls, scans without evidence of dopaminergic deficit (SWEDD), and PSD. With 58,692 photos for training, 11,738 images for validation, and 7826 images for testing, a sizable dataset was used to train the proposed model. With an accuracy of 0.889, recall of 0.9012, precision of 0.9104, and F1-score of 0.9057, the suggested model beats the classification models from the surveyed articles.

Applied to DaTscan pictures, an ensemble of convolutional neural network models, Kurmi, A.[27] presents an ensemble of Deep Learning models for detecting Parkinson's Disease (PD) using DaTscan images. They classified Parkinson's illness using four models—VGG16, ResNet50, Inception-V3, and Xception—and then improved the model's overall performance by using a Fuzzy Fusion logic-based ensemble technique. The Parkinson's Progression Markers Initiative's (PPMI) publicly accessible database is used to assess the suggested model. The suggested model outperforms the individual model in terms of attained recognition accuracy, Precision, Sensitivity, Specificity, and F1-score, which are each 98.45%, 98.84%, 98.84%, 97.67%, and 98.84%, respectively. A GUI-based software tool that rapidly and somewhat accurately detects all classes using magnetic resonance imaging (MRI) has also been created by the authors for public usage. The suggested strategy outperforms existing cutting-edge techniques for detecting PD. Future work by the authors intends to expand their research to include MRI and CT images.

Tarjni Vyas[29] presents a deep learning-based scheme to diagnose Parkinson's disease (PD) using brain images from magnetic resonance imaging (MRI). The authors use two novel approaches using 2D and 3D convolution neural networks (CNN) trained on MRI scans in the axial plane, preprocessed using bias field correction, histogram matching, Z-score normalization, and image resizing. The dataset was collected from Parkinson's progression markers initiative (PPMI). The 3D CNN model achieved a higher accuracy of 88.9% with 0.86 area under the curve (AUC) compared to the 2D CNN model's accuracy of 72.22% with 0.50 AUC. By separating PD patients from healthy controls, the authors come to the conclusion that deep learning models can be employed for early detection. The scientists want to improve the accuracy and other evaluation metric values of the DL model in the future by training the models with GPU parallelization, allowing for more significant sized input in all three dimensions and a greater set of MRI scans in lower times.

Hybrid techniques that combine segmentation and classification techniques were used for the Detection and classification of Neurodegenerative Disorders from MRI images by B. Selvaganesh & R. Ganesan[22]: who proposed a hybrid segmentation and classification technique for detecting neurodegenerative disorders from brain MRI images. The proposed methodology integrates Particle Swarm Optimization (PSO) and Self-Organizing Map (SOM) techniques for efficient image segmentation, followed by Neighbor Intensity Pattern (NIP) feature extraction and integrated Neural Network and K-Nearest Neighbor (KNN) classification techniques for normal and abnormal region classification. The performance was evaluated using two different datasets, ADNI and PPMI, and compared with traditional classification techniques. The results show that the proposed NN-KNN technique outperforms other methods with an accuracy level of 98.6%, sensitivity rate of 95%, specificity rate of 96%, and precision rate of 99.21%. The paper suggests that the proposed framework can be expanded to classify other brain diseases using advanced techniques in the future.

Mahsa Ghorbani and the research team[19] introduce a novel graph convolutional network (GCN) called RA-GCN for disease prediction problems, particularly addressing imbalanced data. Using graph-based classifiers, they proposed a Re-weighted Adversarial Graph Convolutional Network (RA-GCN) to address the class imbalance in disease prediction problems. The proposed method associates a graph-based neural network to each class to weigh the class samples and prevent the classifier from emphasizing any particular class. An adversarial approach trains the parameters of the classifier and weighting networks. The research presents experimental results on synthetic and three publicly available medical datasets to show that RA-GCN is superior to current approaches in determining the patient's state on all three datasets. The research also points out that creating the best graph necessitates enough samples, which can be scarce in datasets with inequities. When the graph is constructed during training, the findings demonstrate that the suggested technique performs better than others. The learned graph from GCN-unweighted is said to have negatively impacted the results of DR-GCN, which is why it performs poorly.

Other studies focus on detecting prodromal Parkinson's disease using fMRI data and deep neural network approaches, like Farhan Shahriar[28], who discuss deep learning techniques to detect Prodromal Parkinson's

Disease (PD) in patients in his paper. The study aims to detect the disease early to alleviate its consequences. The researchers collected fMRI data from 20 Prodromal PD patients and 20 healthy control subjects from the PPMI website. They used deep convolutional neural network architectures to achieve their goal, including mobilenet v1, inception v3, vgg19, and inception resnet v2. They found that the mobile net v1 had the highest classification accuracy of 81.22%, while inception resnet v2, inception v3, vgg19, and ensemble models achieved 75.30%, 62.55%, and 63.32% accuracy, respectively. The study concludes that deep learning techniques can be used to classify image data, even with previously unseen data accurately, and can successfully classify Prodromal PD patients from healthy controls.

As for using Vocal Features extracted from speech signals and employing a random subspace classifier ensemble for classification purposes, some papers like A. Esk Adere, A. Karatutlu, and C. Aenal[30] are working on a study titled "Detection of Parkinson's disease from vocal features using random subspace classifier ensemble," the base classifier utilized by the scientists was the k-NN. There were 1040 record files of 40 people, 40 of whom were healthy and 40 of whom had PD in their dataset, including train and test data. Their work classified people as healthy (class 0) or PD-affected (class 1). They used Matlab to implement all the algorithms, including kNN, LDA, and QDA. They looked at the ideal parameters utilizing an ensemble method called random subspace to improve classification accuracy. Their lowest categorization error rate was 27.65%. And M. Su and K. Chuang[31] developed feature selection for classifying PD speech patterns. Their information was voice-based. The authors used a dataset with two groups. There were 20 participants in the first group of PD sufferers, including six females and 14 males. Ten females and ten males were in the second group, which was in good health. LDA was employed in their paper to assess the effectiveness of feature selection. Jitter, Shimmer, AC NTH, HTN, Median pitch, Mean pitch, Standard deviation, Minimum pitch, Maximum pitch, etc., were only a few features. The authors concluded that fuzzy entropy may be used to eliminate unimportant features.

Despite the many and continuous attempts by researchers to help in the early detection of PD, there are many difficulties and limitations associated with existing detection and screening methods.

Ketna Khanna's[26] discussion and review led the scientists to conclude that a non-invasive, accurate Parkinson's disease screening method is urgently needed. Current methods rely on the observation of symptoms by doctors, which may need to be more accurate and reliable. Several approaches have been proposed using various modalities, but each has limitations, and none can be used in isolation. For instance, PET and SPECT scans are invasive and can cause harm to patients, while FTT and handwritten drawings can only detect upper limb impairments. Voice signals could be more reliable for PD detection. Recently, MRI sequences have been used for PD detection, but their accuracy is still relatively low. Therefore, a more effective and trustworthy method for Parkinson's disease identification with a lower risk of misclassification is urgently needed.

3. METHODOLOGY

a. Data Acquisition and Description:

This section will discuss acquiring the MRI data used in this study. An overview of the data source will be supplied, including the collection method, the number of images obtained, and essential information regarding the data structure and format.

- **Data Source:** The MRI data utilized in this study were gathered from the Parkinson's Progression Markers Initiative (PPMI). The PPMI is a collaborative research effort involving multiple institutions worldwide to accelerate breakthroughs and treatment advancements in Parkinson's disease. As part of this initiative, an open-access data set and biosample library have been established, providing researchers with valuable resources for investigations related to Parkinson's disease.
- **Data Acquisition:** The 3D-T1 MRI data employed in this study consisted of a total of 1,207 images. Specifically, there are 919 MRI scans collected from individuals diagnosed as Parkinson's disease (PD class) and 288 MRI scans from healthy individuals serving as a control group (CN class).

PPMI collected the MRI data using different MRI scanners, including 1.5 Tesla (T) and 3T scanners from multiple vendors. The acquisition protocol followed the standardized protocol developed by the PPMI imaging core, which includes a set of recommended imaging sequences and parameters. The standardized protocol aimed to minimize the variability in data acquisition across different sites and scanners and ensure consistency in data quality.

» **Data Description:**

Each MRI image in the dataset is stored as DICOM format, which is a standard format commonly used in medical imaging.

The MRI images have varying dimensions and resolutions. The exact dimensions depend on the specific scanning parameters used in the acquisition process. The images typically have X pixels in the sagittal plane, Y pixels in the coronal plane, and Z slices in the axial plane to give an overview. The pixel intensities represent the underlying tissue features recorded by the MRI scanner.

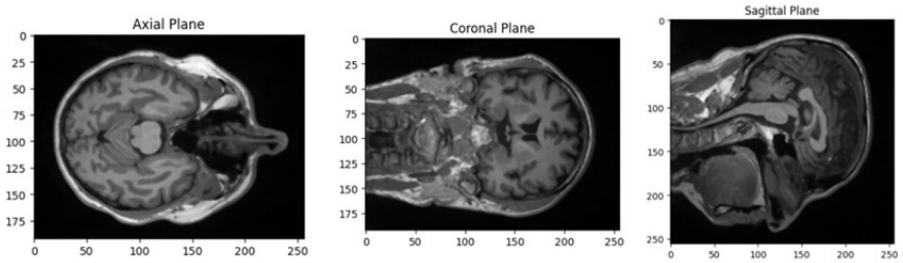

Figure 1. MRI with 3D Dimension

» **Broad demographic:**

The dataset comprises 1,207 images, with 919 MRI scans from individuals with Parkinson's disease and 288 MRI scans from healthy individuals. The dataset includes a broad demographic, incorporating different age groups, sexes, and research groups. This comprehensive dataset provides the basis for a thorough and diversified analysis.

1. Age Distribution

The dataset's subject population's age distribution was assessed. Ages ranging from 60 to 90 were represented by a diversified histogram plot of the age distribution. The biggest peak in the histogram indicates that the bulk of the subjects are between the ages of 60 and 70.

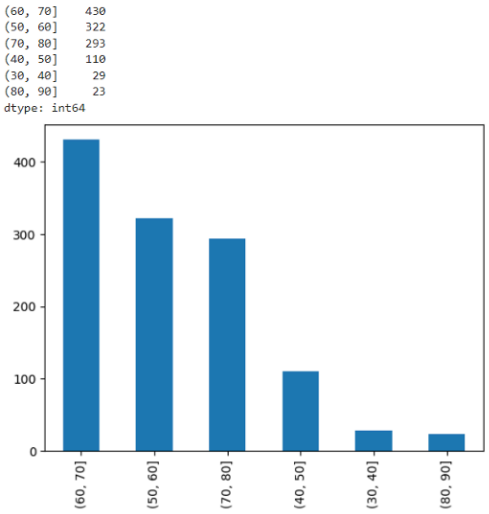

Figure 2. Age Distribution

2. Gender Distribution

The distribution of gender across the dataset was assessed. 32.97% of women and 67.03% of men make up the dataset. This distribution was shown as a bar chart to show the relative proportion of males and females in the dataset.

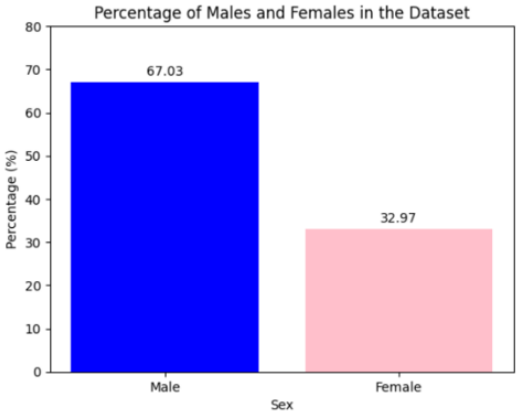

Figure 3. Gender Distribution

3. Research Group Distribution

The dataset contains patients from two different research groups: Control and PD. On a bar graph, numerous subjects in each group were displayed. 919 for PD and 288 for Control.

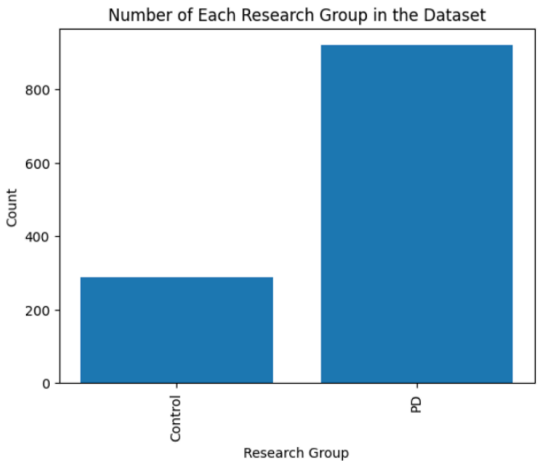

Figure 4. Research Group

4. GENDER DISTRIBUTION IN EACH RESEARCH GROUP

Further, each research group's distribution of males and females was also evaluated. In the dataset, 798 subjects were identified as male and 409 as female. Exciting trends were observed when these totals were broken down by research group. In the control group, there were 182 males and 106 females. This indicates a more excellent representation of males in the control group, although females were also well represented. In contrast, there were 616 males and 303 females within the PD group. This reveals a significantly more significant representation of males in the PD group.

By conducting a detailed statistical analysis of the dataset, we gained valuable insights into the demographic distribution and representation within the dataset. The diverse age and gender representation, along with a broad range of research groups, underscores the comprehensive nature of the dataset. Interestingly, the data reveals that the gender distribution is not uniform across the research groups. Males are overrepresented in both groups and particularly so in the PD group. These insights may have implications for interpreting the results, as gender could be a potential confounding factor.

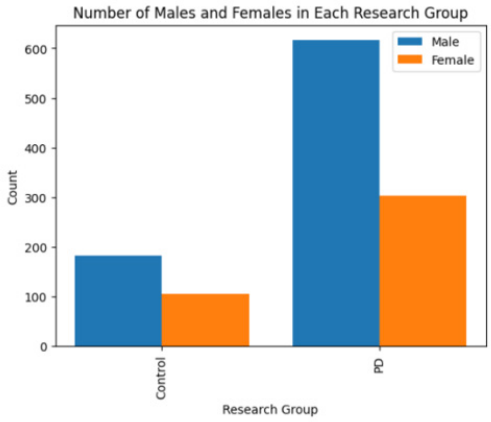

Figure 5. Gender Distribution in Research Groups

4. System Design and Pre-process:

» Work Flow

The project workflow is designed to be sequential yet flexible, allowing for revisions and refinements at each stage based on the observations and results obtained. The following is a step-by-step breakdown of the workflow:

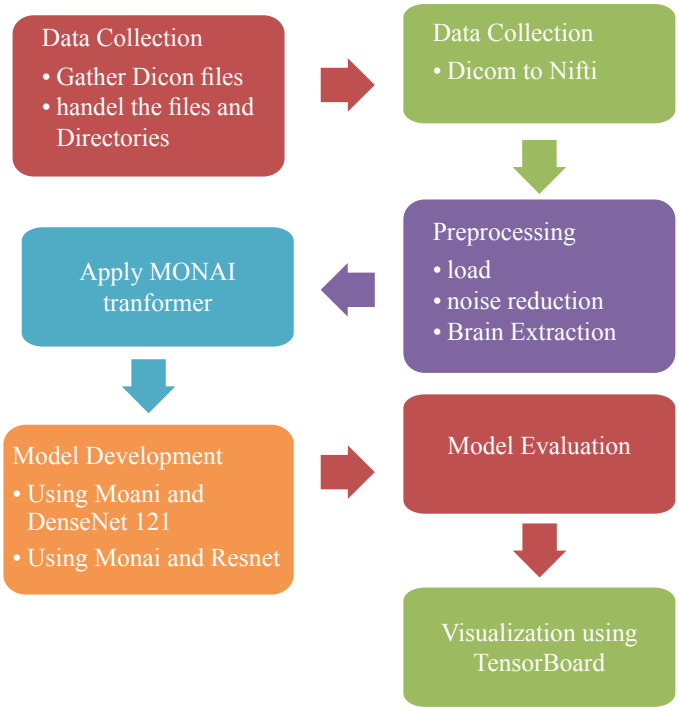

» **Data Collection:**

- Gather the required DICOM files from PPMI

» **Data Conversion:**

- Convert DICOM files to NIFTI format using the dicom2nifti tool for enhanced compatibility with other libraries:

» **Data Preprocessing**

Load and handle the NIFTI files using the Nibabel library and visualize 3D and 2D images.

- **3D visualization:** This is performed using the Nilearn library in Python, which is specifically designed for neuroimaging data analysis.

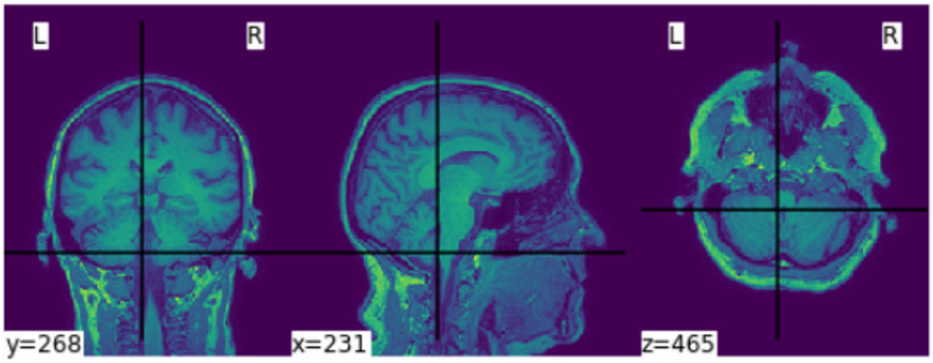

Figure 6. NIFTI file with 3D visualization

- **2D visualization:** Matplotlib is a powerful and flexible Python library for creating static, animated, and interactive visualizations

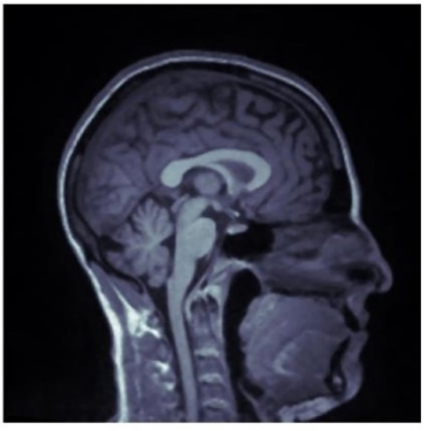

Figure 7. NIFTI file with 2D visualization

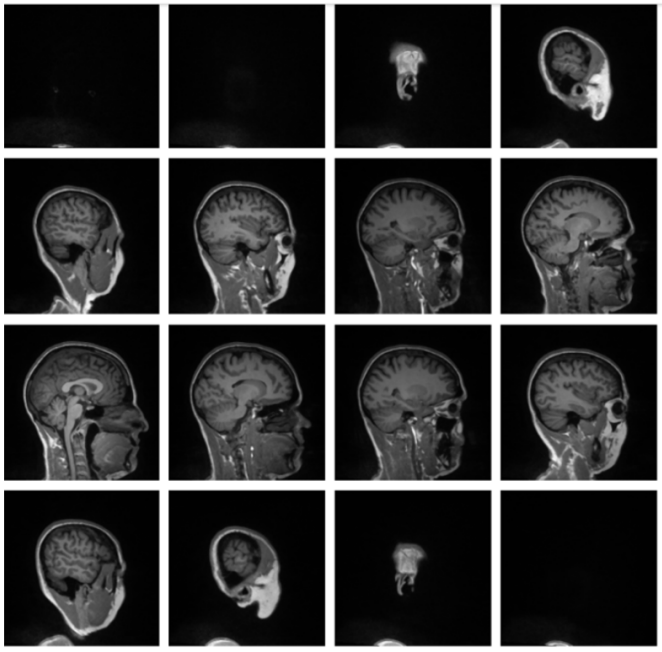

Figure 8. Series of 2D visualization for nifti file

» **Apply noise reduction filters using the 'scipy.ndimage.filters' module**

» **Applying Median Filter and Creating New NIfTI Files:**

To process the neuroimaging data, we use a Python script that applies a median filter to each NIfTI file in the input directory. The median filter is used to reduce noise and smooth the image. The size parameter is set to 3, indicating that the filter should consider a 3x3x3 neighborhood around each voxel (3D pixel) to calculate the median value.

The result if noise reduction is shown in the next figure.

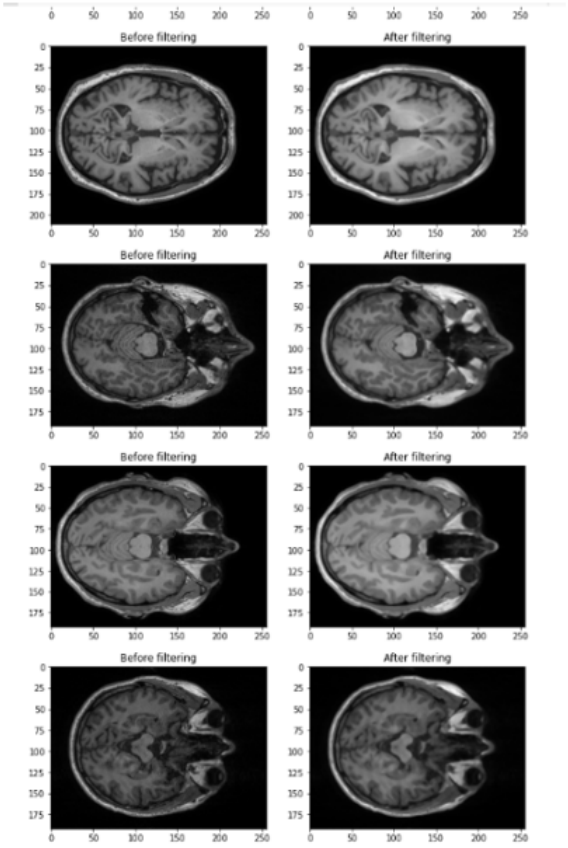

Figure 9. Noise reduction, Before and After

» **Execute brain extraction in the neuroimages with the BrainExtractor tool to focus on relevant regions for analysis and reduce data dimensionality**

In this part of the process, we perform a key pre-processing step in neuroimaging analysis, '**brain extraction'**, which is the process of removing non-brain tissue from an image of the brain. Here we make comparison before and after applying Brain Extraction process.

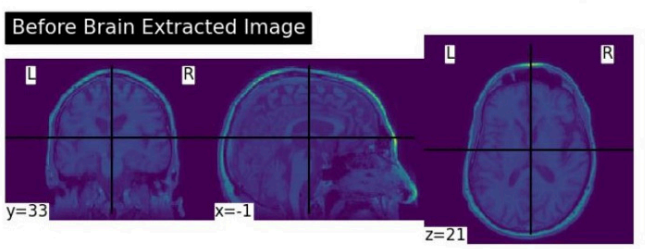

Figure 10. before brain extration process

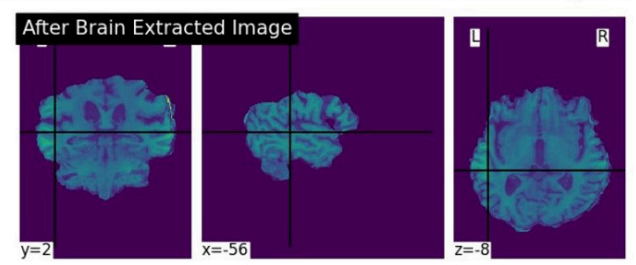

Figure 11. After Brain Extraction process

5. MODEL IMPLEMENTATION, TRAINING AND EVALUATION

This section focuses on implementing, training, and evaluating CNN-based models for the binary classification of PD using MRI data. Specifically, two popular CNN architectures, DenseNet121 and ResNet, are utilized in this study. These architectures have demonstrated strong performance in various computer vision tasks, including medical image analysis.

The MONAI (Medical Open Network for AI) architecture is employed to simplify the implementation and training process.

Transfer Learning, a powerful technique in deep learning, is also explored in this section. The models can capture rich and abstract image features by leveraging pre-trained models, such as DenseNet121 and ResNet, trained on large-scale datasets like ImageNet. Transfer Learning allows the models to be fine-tuned on the specific task of PD classification with limited labeled medical imaging data. This approach reduces the computational burden and enhances the model's generalization capabilities.

The data pre-processing includes intensity normalization, resizing, and augmentation techniques such as rotation, flipping, and random transformations. These pre-processing techniques ensure the input data

is standardized and contains sufficient variability for the models to learn meaningful patterns and generalize well.

The training process involves iteratively feeding the pre-processed data into the DenseNet121 and ResNet models and updating their parameters to minimize classification loss. The models are trained using a labeled dataset of MRI scans from PD patients and healthy controls. The training progress is monitored by tracking the loss function and validation accuracy. Early stopping techniques may be employed to prevent overfitting and determine the optimal number of epochs.

Evaluation metrics such as accuracy and F1-score assess the models' classification performance.

By implementing and training DenseNet121 and ResNet models using the MONAI framework, this section aims to comprehensively understand their performance for binary classification of PD using MRI data. The results and analysis obtained from this study can contribute to developing accurate and reliable tools for the early recognition and diagnosis of Parkinson's Disease.

Software Environment:

```
[4]  monai.config.print_config()
     logging.basicConfig(stream=sys.stdout, level=logging.INFO)

MONAI version: 1.1.0
Numpy version: 1.22.4
Pytorch version: 2.0.1+cu118
MONAI flags: HAS_EXT = False, USE_COMPILED = False, USE_META_DICT = False
MONAI rev id: a2ec3752f54bfc3b40e7952234fbeb5452ed63e3
MONAI __file__: /usr/local/lib/python3.10/dist-packages/monai/__init__.py

Optional dependencies:
Pytorch Ignite version: 0.4.12
Nibabel version: 3.0.2
scikit-image version: 0.19.3
Pillow version: 8.4.0
Tensorboard version: 2.12.2
gdown version: 4.6.6
TorchVision version: 0.15.2+cu118
tqdm version: 4.65.0
lmdb version: NOT INSTALLED or UNKNOWN VERSION.
psutil version: 5.9.5
pandas version: 1.5.3
einops version: NOT INSTALLED or UNKNOWN VERSION.
transformers version: NOT INSTALLED or UNKNOWN VERSION.
mlflow version: NOT INSTALLED or UNKNOWN VERSION.
pynrrd version: NOT INSTALLED or UNKNOWN VERSION.

For details about installing the optional dependencies, please visit:
    https://docs.monai.io/en/latest/installation.html#installing-the-recommended-dependencies
```

Figure 12. MONAI library configuration

As shown in the above figure, we used MONAI library version 1.1.0 for developing the AI module. This information is significant for reproducibility and ensuring that the code is compatible with the expected MONAI functionalities.

The figure also lists optional dependencies that are used alongside MONAI. Such as: PyTorch Ignite version 0.4.12. Nibabel version 3.0.2. scikit-image version 0.19.3, Pillow version 8.4.0. Tensorboard version 2.12.2, gdown version 4.6.6. TorchVision version 0.15.2+cu118. tqdm version 4.65.0:. Additionally, the output mentions the versions of other optional dependencies, such as lmdb, psutil, pandas, einops, transformers, mlflow, and pynrrd. These dependencies might not be installed or their versions are not known.

» **Load the dataset and split it:**

At this point we begin with preparing our dataset for training and validation.

loads the dataset, assigns appropriate labels to the images based on their filenames, stores the file paths and labels in separate lists, and converts the labels to NumPy arrays for further processing in the model implementation and evaluation phases.

» **Define Transformers, Datasets and DataLoaders:**

This part is responsible for defining the transformers, datasets, and data loaders for the training and validation sets:

□ Two sets of transforms are defined: train_transforms and val_transforms.

o train_transforms is a composition of transformations including: ScaleIntensity, EnsureChannelFirst, Resize images to a specified shape of (96, 96, 96), RandRotate90.

o val_transforms is a composition of transformations similar to train_transforms, excluding the RandRotate90 transformation.

□ A dataset and a data loader are created for checking the first batch of all the dataset, and then for train and validation datasets seperatlly. With a **batch size** of **16**, shuffling the data, 2 worker processes for data loading, and memory pinning if CUDA is available

» **Model Architecture**

We used two architectures in our study: (ResNet and DenseNet121)

- **ResNet:** The model used is a variant of the ResNet (Residual Network) architecture, specifically designed for 3D image classification tasks. Here are more details about the model:

- **Basic ResNet**: The ResNet variant used is referred to as "**basic**". It consists of four stages, each containing multiple residual blocks. The number of residual blocks in each stage is defined by the layers parameter. In this case, the layers list is set to [1, 1, 1, 1], indicating one residual block in each stage. And the number planes channels for each residual block in the respective stages is set to [64, 128, 256, 512], The **spatial dimensions** of the input data is set to 3, indicating that the input data is 3D volumetric data. The number of input channels in the input data. is set to 1, indicating **grayscale** images. And the output class number is 2, representing the **binary classification** task of distinguishing between individuals with PD and healthy controls.
- **DenseNet121:** It is a variant of the DenseNet architecture, specifically designed for 3D image analysis. DenseNet architectures have gained popularity due to their effectiveness in capturing intricate patterns and features from images.
- The **DenseNet121** model consists of **121 layers**, making it a relatively deep network. It is specifically designed for spatial dimensions of 3, which indicates that it is suitable for processing 3D volumetric data, such as MRI scans.
- The input to the DenseNet121 model is an MRI image with a single channel is set to 1, this is typical for **grayscale** images. The output of the DenseNet121 model is a 2-channel output.

» **Loss Function**

The loss function used is **CrossEntropyLoss**. It is a commonly used loss function for multi-class classification tasks, including binary classification as a special case.

The **CrossEntropyLoss** function combines both the **softmax** activation and the negative log likelihood loss in a single operation. It encourages the model to assign high probabilities to the correct class and low probabilities to the incorrect class.

In the specific context of Parkinson's Disease classification, the model's output is a probability distribution over the two classes: PD and healthy controls. The **CrossEntropyLoss** function takes this probability distribution and the corresponding ground truth labels as inputs. It computes the loss by comparing the predicted probabilities with the true labels, taking into account both the correct and incorrect predictions.

The use of **CrossEntropyLoss** as the loss function is appropriate for training the model to optimize the parameters based on minimizing the classification error. By minimizing the loss, the model learns to improve its predictions and make more accurate classifications.

» **Optimizer:**

The optimizer used is **Adam**. the Adam optimizer is instantiated with the model's parameters as the input. By passing '**model.parameters()'** as an argument, the optimizer is aware of the model's learnable parameters (weights and biases) that need to be updated.

The **learning rate**, specified as **1e-5**, determines the **step size** at which the optimizer adjusts the model's parameters during each update. A smaller learning rate typically leads to slower but more precise convergence, while a larger learning rate may result in faster convergence but with the risk of overshooting the optimal solution.

» **Training :**

□ Before the training process **is begin,** we indicate the validation step to be performed every 2 epochs, and the best metric value obtained during training initialized to -1, this will be used to track the best metrics through the training process. And '**SummaryWriter' is used** to visualize and log the training process. The maximum number of epochs is set to 100. Early stopping technique was used. Two empty lists, '**epoch_loss_values'** and '**metric_values'**, are created to store the epoch-wise loss values and metrics, respectively.

□Then the training loop begins with a loop over each epoch. Within each epoch, the model is set to training mode. And **epoch loss** is initialized to **0** to calculate the average loss for the current epoch. A **step** variable is introduced to track the progress within the epoch.

□The loop iterates over the batches of data in the **train loader**. After completing the epoch, the **average loss** is calculated.

□Then the model is set to evaluation mode. Where the validation loop is performed if the current epoch number plus one is divisible by **validation interval**. The loop iterates over the batches of data in the **validation loader**.

In this process we implement the training loop for a model using the MONAI framework. Performs forward and backward passes, updates the model's parameters using the Adam optimizer, and tracks the training and

validation metrics. The training process continues for a maximum number of epochs while monitoring the validation metric for potential early stopping.

» **Result and Discussion:**

The Accuracy and F1 score were calculated as evaluation metrics for the model performance, comparing the two results for two models (ResNet and DenseNet121) and decides which is the best.

- **ResNet**

```
  warnings.warn(f"Modifying image pixdim from {pixdim} t
/usr/local/lib/python3.10/dist-packages/monai/data/utils
  warnings.warn(f"Modifying image pixdim from {pixdim} t
Accuracy: 0.9250
F1 score: 0.9247
```

  - **Accuracy: 0.9250**
  - **F1 Score: 0.9247**

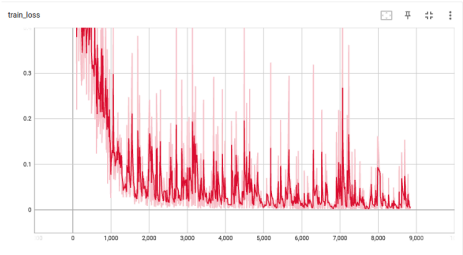

Figure 13. ResNet train loss

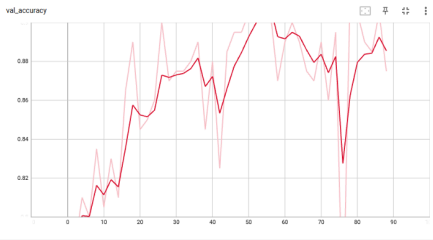

Figure 14. ResNet Validation accuracy

The ResNet model achieved an accuracy of 0.9250, indicating that it correctly classified 92.50% of the instances in the validation set. The F1 score of 0.9247 suggests a balanced performance in terms of precision and recall.

- **DenseNet**

```
  warnings.warn(f"Modifying
Accuracy: 0.8850
F1 score: 0.8847
```

  - **Accuracy: 0.8850**
  - **F1 Score: 0.8847**

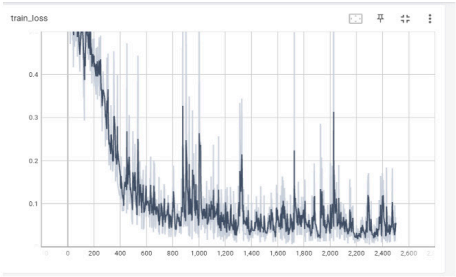

Figure 15. DenseNet121 train loss

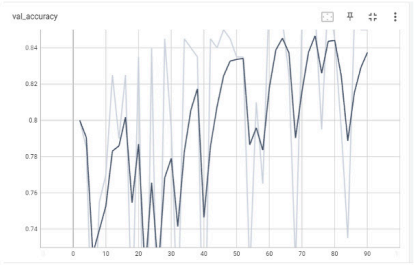

Figure 16. DenseNet121 validation accuracy

The DenseNet121 model achieved an accuracy of 0.8850, correctly classifying 88.50% of the instances in the validation set. The F1 score of 0.8847 indicates a balanced performance between precision and recall.

Comparing the two models:

□ The ResNet model outperformed the DenseNet121 model in terms of accuracy, achieving a higher accuracy of 0.9250 compared to 0.8850 for DenseNet121.

□ The F1 score for ResNet (0.9247) is slightly higher than DenseNet121 (0.8847), indicating that the ResNet model achieved a better balance between precision and recall.

It is important to note that these results are specific to the dataset and problem at hand. The ResNet model demonstrates a superior ability to classify Parkinson's disease based on MRI Nifti files compared to DenseNet121.

Further analysis and discussion based on the points you mentioned:

1. **Interpretation of Accuracy and F1 Scores:**

a. The accuracy and F1 scores provide an evaluation of the model's performance in classifying Parkinson's Disease from MRI Nifti files.

b. A high accuracy (0.9250 for ResNet) indicates that the model can correctly identify Parkinson's Disease cases, which is crucial for early diagnosis.

c. The F1 score (0.9247 for ResNet) considers both precision and recall, providing a balanced measure of the model's ability to classify both Parkinson's Disease and non-Parkinson's Disease cases.

d. These scores demonstrate the potential of the model to aid in the early detection of Parkinson's Disease, allowing for timely intervention and treatment.

2. **Reasons for Superior Performance of ResNet:**

a. ResNet's deeper architecture and skip connections contribute to its superior performance.

b. Deeper architectures enable the model to learn more complex patterns and capture finer details from the MRI images.

c. Skip connections allow for better gradient flow during training, alleviating the vanishing gradient problem and facilitating the optimization process.

d. The combination of these factors enables ResNet to extract and leverage meaningful features for accurate classification, leading to its superior performance compared to DenseNet121.

6. CONCLUSION

Parkinson's Disease (PD) is a neurodegenerative disorder characterized by motor symptoms such as tremors, bradykinesia, and rigidity. So an early and accurate diagnosis of this disease is crucial for effective treatment and management of the disease. The disease is diagnosed using many different ways, and the most important prominent and most accurate of which is Magnetic Resonance Imaging (MRI) has emerged as a promising modality for analysing brain structures and detecting neurodegenerative diseases.

Using MRI, This study has implemented two binary classification models to distinguish between individuals with PD and healthy controls. By employing PyTorch, and MONAI to design, implement, and training of deep learning models. Transfer learning Techniques also used to implement DenseNet121 and ResNet architectures, leveraging their proven effectiveness in image classification tasks.

While this study achieved high accuracy and F1 score, ResNet outperformed DenseNet121, reaching an accuracy of 0.9250 and F1 Score of 0.9247, where the accuracy in DenseNet was 0.8850 and F1 score 0.8847. This result showcases the efficacy of ResNet in PD classification tasks. The results of this work advance the use of MRI and deep learning methods for PD diagnosis. We think that these discoveries could lead to useful clinical applications that would ultimately help those who have Parkinson's disease and facilitate early diagnosis and treatment.

Looking forward, we plan to expand our research by exploring different model architectures: Apart from ResNet and DenseNet, like Inception,

VGG, or EfficientNet to identify the most suitable architecture for Parkinson's Disease classification. Additionally we will incorporate various data augmentation techniques such as translations, or elastic deformations, which could enhance the models' ability to generalize to unseen variations in the MRI images. And to perform better and improve model performance and generalization skills, we may give our models more varied examples to learn from by expanding the training dataset, which may.

By the end of this work, we are hopeful that further investigation and study in this field will advance the diagnosis and treatment of Parkinson's disease, bringing us closer to better patient outcomes and higher standards of living.

REFERENCES

[1] Computer Vision Technique for Neuro-image Analysis in Neurodegenerative Diseases: A survey " prepared by : Yusera Farooq khan , Baijnath Kaushik , published by : AISSMS Institute of Information Technology, Pune, India. Mar 12-14, 2020

[2] Classification of Parkinson's Disease Using MRI Data and Deep Learning Convolution Neural Networks" prepared by: Roshni Saha.

[3] Densely Connected Convolutional Networks'' Gao Huang, Zhuang Liu, and Laurens van der Maaten

[4] mplementing Magnetic Resonance Imaging Brain Disorder Classification via AlexNet–Quantum Learning'', BY: Naif Alsharabi, Tayyaba Shahwar, Ateeq Ur Rehman, Yasser Alharbi.

[5] Association, A. Alzheimer's disease facts and figures. Alzheimer's Dement. **2017**, 13, 325–373.

[6] Implementing Magnetic Resonance Imaging Brain Disorder Classification via AlexNet–Quantum Learning

[7] Detection of Parkinson's Disease from 3T T1 Weighted MRI Scans Using 3D Convolutional Neural Network

[8] 3D Convolutional Neural Networks for Classification of Alzheimer's and Parkinson's Disease with T1-Weighted Brain MRI

[9] A Deep Learning Method to Detect Parkinson's Disease from MRI Slices

[10] Prostate Cancer Classifier based on Three-Dimensional Magnetic Resonance Imaging and Convolutional Neural Networks, 2023

[11] Graph Theoretical Metrics and Machine Learning for Diagnosis of Parkinson's Disease Using rs-Fmri

[12] PARKINSON'S DISEASE DETECTION Using FMRI Images LEVERAGIN transfer learning on CONVOLUTIONAL NEURAL NETWORK

[13] Predicting diagnosis 4 years prior to Alzheimer's disease incident

[14] Parkinson's Disease Classification from Magnetic Resonance Images (MRI) using Deep Transfer Learned Convolutional Neural Networks

[15] Computer Vision Technique for Neuro-image Analysis in Neurodegenerative Diseases:A survey

[16] A Hospital Application Involving Deep Learning Architecture for Detecting Parkinson's Disease

[17] A Deep Approach to Quantify Iron Accumulation in the DGM Structures of the Brain in Degenerative Parkinsonian Disorders Using Automated Segmentation Algorithm

[18] Detection of Parkinson's Disease from Neuro-imagery using Deep Neural Network with Transfer Learning

[19] Bayesian Optimization with Support Vector Machine Model for PD classification

[20] Mahsa Ghorbani , Anees Kazi, Mahdieh Soleymani Baghshah, Hamid R. Rabiee, Nassir Navab, RA-GCN: Graph Convolutional Network for Disease Prediction Problems with Imbalanced Data(2022), https://doi.org/10.1016/j.media.2021.102272

[21] Çağatay Berke Erdaş, Emre Sümer , A Deep Learning Method to Detect Parkinson's Disease from MRI Slices, SN Computer Science (2022) 3:120, https://doi.org/10.1007/s42979-022-01018-y

[22] Anupama Bhan, Sona Kapoor, Manan Gulati, Ayush Goyal, "Early Diagnosis of Parkinson's Disease in brain MRI Using Deep Learning Algorithm" , IEEE Xplore Part Number: CFP21ONG-ART; 978-0-7381-1183-4

[23] B. Selvaganesh & R. Ganesan, "A hybrid segmentation and classification techniques for detecting the neurodegenerative disorder from brain Magnetic Resonance Images", Multimedia Tools and Applications (2022) 81:28801–28822, https://doi.org/10.1007/s11042-022-12967-0

[24] Sabyasachi Chakraborty, Satyabrata Aich, and Hee-Cheol Kim, "Detection of Parkinson's Disease from 3T T1 Weighted MRI Scans

Using 3D Convolutional Neural Network" , Diagnostics 2020, 10, 402; doi:10.3390/diagnostics10060402

[25] Roshni Saha, "Classification of Parkinson's Disease Using MRI Data and Deep Learning Convolution Neural Networks", Iowa State University 2019.

[26] Jigna Hathaliya, Nisarg Patel, Rajesh Gupta, and Sudeep Tanwar, " Convolutional Neural Network-Based Parkinson Disease Classification Using SPECT Imaging Data" DOI: 10.3390/math10152566

[27] Ketna Khanna, Sapna Gambhir, Mohit Gambhir, "CURRENT CHALLENGES IN DETECTION OF PARKINSON'S DISEASE" JOURNAL OF CRITICAL REVIEWS, ISSN- 2394-5125, VOL 7, ISSUE 18, 2020

[28] Kurmi, A.; Biswas, S.; Sen, S.; Sinitca, A.; Kaplun, D.; Sarkar, R. "An Ensemble of CNN Models for Parkinson's Disease Detection Using DaTscan Images". Diagnostics 2022, 12, 1173. https://doi.org/10.3390/diagnostics12051173

[29] Farhan Shahriar, Amarttya Prasad Dey, Naimur Rahman, Zarin Tasnim, &Mohammad Zubayer Tanvir, "Detection of Prodromal Parkinson's Disease with fMRI data and deep neural network approaches" 2021. Brac University

[30] Tarjni Vyas, Raj Yadav, Chitra Solanki, Rutvi Darji, Shivani Desai, & Sudeep Tanwar, " Deep learning-based scheme to diagnose Parkinson's disease" Expert Systems. 2022;39:e12739. https://doi.org/10.1111/exsy.12739

[31] A. Esk Adere, A. Karatutlu, and C. Aenal, "Detection of parkinson's disease from vocal features using random subspace classifier ensemble", in 2015 Twelve International Conference on Electronics Computer and Computation (ICECCO), 2015, pp. 1-4.

[32] M. Su and K. Chuang, " Dynamic feature selection for detecting parkinson's disease through voice signal", in 2015 IEEE MTT-S 2015 International Microwave Workshop Series on RF and Wireless Technologies for Biomedical and Healthcare Applications (IMWS-BIO), 2015, pp. 148-149.

[33] Gao Huang, Zhuang Liu, Laurens van der Maaten, and Kilian Q. Weinberger in their paper "Densely Connected Convolutional Networks" in 2016.

[34] Kaiming He, Xiangyu Zhang, Shaoqing Ren, and Jian Sun in their paper "Deep Residual Learning for Image Recognition" in 2015.

[35] Provision For The Object Of The Procurement Is The Acquisition Of The Rtk Correction Signal Needed For The Tasks Of The E And Y Responsibility Areas Of The Ely Centers. [Tender documents : T487733908]. (2023, April 29). MENA Report.

[36] New gene therapy to stop Parkinson's disease? - Longevity.Technology - Latest News, Opinions, Analysis and Research. https://longevity.technology/news/new-gene-therapy-can-stop-parkinsons-disease-before-it-even-starts/

[37] Dopamine induces soluble α-synuclein oligomers and nigrostriatal degeneration — Northwestern Scholars.

[38] https://www.scholars.northwestern.edu/en/publications/dopamine-induces-soluble-%CE%B1-synuclein-oligomers-and-nigrostriatal-

[39] Reproductive factors and Parkinson's disease risk in Danish women.. https://escholarship.org/uc/item/70x8t3bs

[40] United States : AbbVie Receives European Commission Approval of RINVOQ (upadacitinib) for the Treatment of Adults with Moderate to Severe Active Rheumatoid Arthritis. (2019). MENA Report.

[41] Awakening Dormant Neurons May Lead to Disease-Modifying PD Therapy, Early Study Claims. https://parkinsonsnewstoday.com/news/awakening-dormant-neurons-could-provide-disease-modifying-parkinsons-treatment-animal-study/

Research Article

Mechatronic System Design of Feeding Mechanism in Shuttlecock Launcher by using Rotary to Linear Motion

Ali Doraghi[1*]

[1]*Department of Mechanical Engineering, Islamic Azad University, Khomein, Iran*
**E-mail address: alidoraghi1994@gmail.com*

ABSTRACT

Taking advantage of one of the most common mechanical mechanism that we called it Rotary to Linear motion into one of the common popular gym interest apparatuses named shuttlecock launcher Machine to improve and promote their ability and keep it apart from complexity in a particular part has been addressed. This paper described and designed the Rotary to Linear motion into the Feeding Mechanism Unit one of the most important parts in the shuttlecock launcher that will push the shuttlecocks in the dispenser unit through the ejection unit.

Keywords*: Shuttlecock Launcher, Mechatronic System, Feeding Mechanism, Mechanical Design.*

1. INTRODUCTION

In the world of machine controls, linear motion is the name given to the process of moving some object in a straight line, usually with a programmed speed and to a defined position, in addition to the mechanical components, the linear-motion control system may include control electronics to process movement commands into motor-control commands and sensors to provide position feedback to the control system [1]. Most industries using technical and twist processes and create mechatronic systems and to produce superfluous quantities and save more time and cost at the same time. This obviously, human life becomes more rapidly and optimizing when taking advantage of the mechatronic systems. These technologies advances are highly supported by the development of mechatronic, the miniaturization and the drastic cost reduction of smart sensors and actuators, and of course the increased processing capacity [2]. Briefly, the feeding mechanism one of the common systems which led to process optimizing in systems such as training with shuttlecocks in badminton gym. A wide variety of ball throwing machines employing counter rotating wheels have been used in the past for activities such as tennis, ping pong, baseball, and volleyball practice [3]. Gym industrials one of the common that automation machines have been advancing during past decades, like badminton gym facilities. it is difficult to practice badminton without the assistance of another skilled player and coaches [4]. Shuttlecock launcher is a machine that will help the badminton trainer with assistance, and it is highly accepted. However, this kind of feeding mechanism will be used by ping pong ball machines for feeding purposes or any other fields that call for feeding mechanism purposes. Shuttlecock launcher includes three major units, Ejection Unit, Feeding Mechanism Unit, and Dispenser Unit. In this paper, we will describe and map the new kind of feeding mechanism out that we called FMU.

2. MECHANISM PERFORMANCE IDENTIFICATION

Different feeding mechanisms have been designed in the shuttlecock launcher machine, includes gripper mechanisms or railing mechanisms, that pushing a shuttlecock with complexity and cost. However, I have addressed this kind of mechanism in a specific and simple design. We can use this kind of mechanism for different purposes through different parts. The shuttlecock launcher machine includes a dispenser unit, a feeding mechanism unit, and an ejection unit. As I mentioned, in this paper, I am going to map the Feeding mechanism unit out. The feeding mechanism

Unit (FMU) transmits and pushing the shuttlecocks from the dispenser unit into the ejection unit, and the ejection unit has a main role in order to eject and proper the shuttlecocks.

As I mentioned, guide and push the shuttlecocks from the dispenser unit through the ejection unit will be done by FMU, which plays a key role in the machine performances. So basically, to push the shuttlecocks out it calls for the design of a mechanical mechanism that can cope with this mission, and for this reason, I have chosen a kind of Rotary to Linear motion mechanism and going to use it in the FMU structure. In continuity, the purpose of this article will be in touch and focus on the FMU structure and design it.

3. FMU STRUCTURE & DESIGN

In order to design and setting the FMU efficient system, it is calls for investigating the FMU roles in the machine. As I mentioned, the shuttlecock launcher machines taking advantage of the FMU in order to push shuttlecocks into the ejection unit. Moreover, we need a mechanism that can carry or push shuttlecocks one by one through the dispenser unit, efficiently.

To do this approach, I have taken advantage of one of the most popular mechanisms that will convert the Rotary motion to Linear motion with simple assembly parts. Convert the Rotary motion to the Linear motion has been done by the specific components that we should recognize the components part by part. In order to do this design, DC- Gearbox Motor (4), Belt-Wheel (2), Thread-Shaft (1), have been used in the FMU structure.

DC-Gearbox Motor has been used for the FMU kinematic power with 200 RPM, Belt-Wheel for power transmit through Belt-Wheel, and then, a Thread-Shaft for the linear motion on behalf of kinematic power when transmit by Belt-Wheel. However, in this structure, we have more components like hard surfaces (3,5,6) to keep the parts touch. (Fig.1)

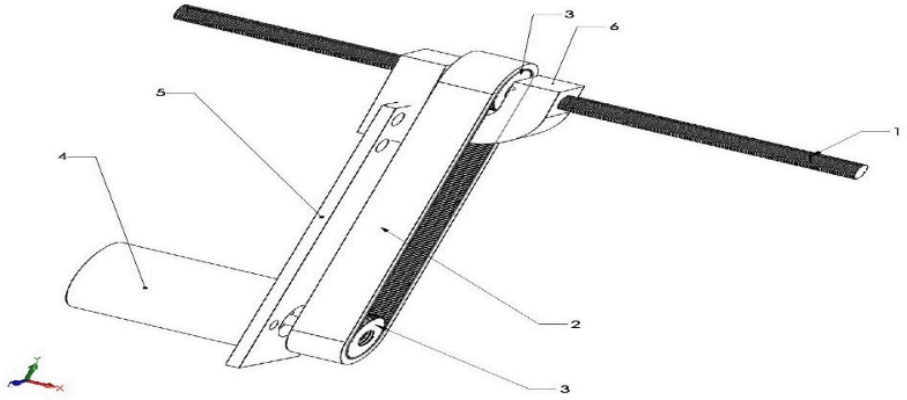

Figure 1. As I mentioned, the FMU has the main function of feeding the machine.

With DC-Gearbox Motor circulation, the whole of the system will run in a circle direction which led to Thread-Shaft circulate-reciprocal motions due to the thread that exists on the shaft surface. Besides, no matter what component scales will use in this kind of mechanism, we can use any scales to design this kind of mechanism. While the thread-shaft (1) movement due to the Belt-Wheel circulation, it will touch the shuttlecock surface (Fig2), and push or force one, and in continuity, all the rest shuttlecocks will be getting out one by one in dispenser unit (11) through ejection unit. (Fig.2)

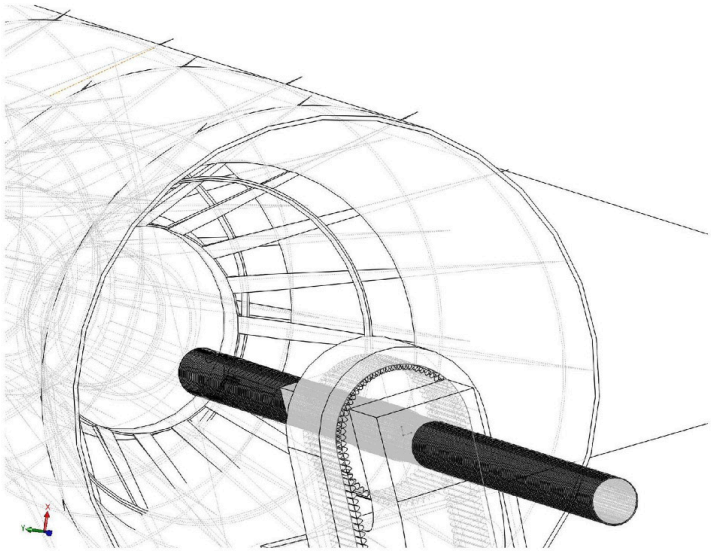

Figure 2. The Belt-Wheel circulation.

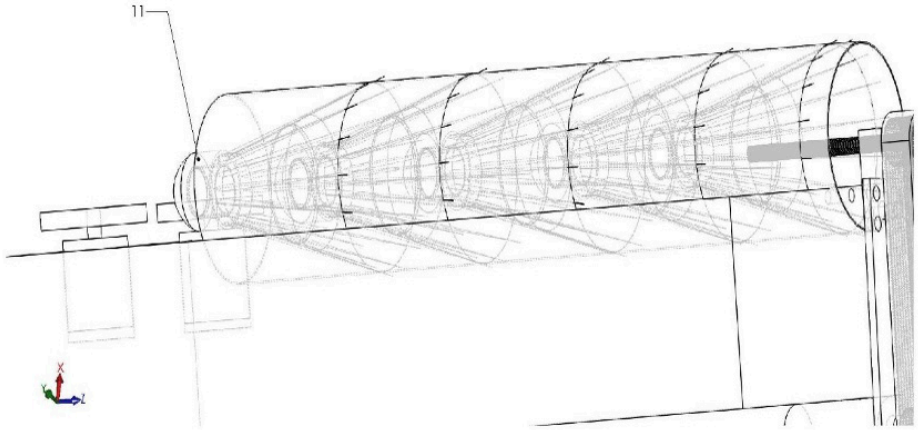

Figure 3. The dispenser depletion of shuttlecocks

Hence, the thread-shaft will push back by reverse motor circulation with the dispenser depletion of shuttlecocks. (Fig.3)

1. FMU REPAIR AND MAINTENANCE

The FMU has been innovated by very simple components and structural. basically, the more simples one mechanism is, the more can keep it running. As we know, we can take advantage of Lubrication and cleaning for maintenance.

2. CONCLUSION

As the result, we have developed and designed one of the most popular mechanical-Mechanism movements in a shuttlecock launcher machine with very simple components and assembly, that can push shuttlecocks efficiently and simply. Moreover, the unique of Rotary-to-Linear motion converter design proposed here can be applied to various engineering fields, instead of existing mechanical Rotary-to-Linear mechanisms, due to the advantages in a compact size and precise control.

REFERENCES

[1]Tom Stevic, How to transform rotary motion into linear, Jun 21, 2018

[2]S. Bover iea, Dongil Dan Cho b, H. Hashimotoc, M. Tomizukad, WangWeie, D. Zühlkef: Mechatronics, robotics and components for automation and control, IFAC milestone report, 25,April, 2016

[3]Jonathan Taryoto, US6752138B2: Shuttlecock launcher and method for launching, 2004,06,22

[4]A.P.G. De Alwis ; Chanaka Dehikumbura ; Mahesh Konthawardana ; T. D. Lalitharatne ; V.

[5]P. C. Dassanayake: Design and Development of a Badminton Shuttlecock Feeding Machine to Reproduce Actual Badminton Shots, 2020 5th International Conference on Control and Robotics Engineering (ICCRE), 24-26 April 2020

Research Article

Effect of Stacking Sequence on The Mechanical Performance of Hybrid Fiber Reinforced Epoxy-Polyester Composites

Fayçal Mili[1,2,*], Sarah Guenifa[1,2], Toufik Achour[1,2]
[1]*Department of Mechanical Engineering, Mentouri Brothers' University, Constantine, Algeria*
[2]*Laboratory of Mechanics, Mentouri Brothers' University, Constantine, Algeria*
[*]*E-mail address: mili.faycal@umc.edu.dz, mili_faycal@yahoo.fr,*
0009-0001-3654-0020, 0000-0002-7822-9118

ABSTRACT

The main aim of this present investigation is to evaluate mechanical properties of different hybrid laminates prepared with different combinations of fiber and resin. The impregnation of laminates is done by epoxy and polyester resin as matrix material. Various structures under tensile strength were considered with different combinations glass, carbon fibers reinforced epoxy-polyester resin laminates. The current research work reveals the effect of stacking sequence on the mechanical behavior of symmetric laminated composites. They are composed ofthree layers alternated between +□/-□, +□/0° and +□/90° forming respectively balanced and angle ply laminates. Thus, it is important to study the performance of this composites in order to assess their failure mechanism. In this paper, analytical predictions were performed based in developing failure criteria for unidirectional fiber composites. The changes of stacking sequences have significant effect on the tensile properties and on the development of cracks likewise. The analysis reveals that the net effect is dependent on the anisotropy of the fiber. Under evaluation of the mechanical behavior of the combined matrix materials, the fibers may have a detrimental effect on strength.

Keywords: *Composite, Hybrid, Combined Matrix, Tensile, Failure.*

1.INTRODUCTION

Composite materials have been widely utilized in many industries, due to their high strength and stiffness to weight ratios. As the reinforcement was the strength source, it is preferable in certain applications to combine several fibers of various natures to constitute hybrid materials. Knowledge of the mechanical behavior of the composite material prevents its failure, improves its manufacturing processes and solves its life problems.

Hybrid composite materials not only represent a new field of fundamental research in which the creativity of the mechanic can be fully expressed to develop new materials, but they also allow, through their new and remarkable properties associated with their multi-functionality, the emergence innovative industrial applications in extremely varied fields. In terms of applications, hybrids are invading the field of transport. Their use has permitted to optimize the mechanical performance of vehicles and therefore reduce their fuel consumption. Consideration of the layer stacking sequence has a significant influence on the behavior and properties of hybrid laminates.

Theoretical and experimental research on the mechanics of composite materials have permitted to propose resistance criteria developed either by the approach of micromechanics [1,2], or by that of macromechanics [3,4]. In the first, the failure criteria are established by considering the mechanical properties of the constituents of the material and of the interfaces. Nalla Mohamed and Praveen Kumar [5] have varied the mixed fiber volume fraction (carbon-glass) of a composite structure in order to obtain a gain on the failure strength, a stiffness increase and a noticeable lightening for a reduced cost. A Numerical study (Finite Element Method) is developed for fiber reinforced composite tubes using Hashin's criteria and the initiations of intra-laminar failures are identified. On theother hand, experimental studies are carried by Pandya et al. [6] under both tensile and compressive in-plane quasi- static loading for two types of hybrid composites made by using satin weave carbon fabrics and plain weave E-glass fabrics with epoxy resin. Furthermore, Abedi et al. [7] have used finite element modeling to investigate the energy absorption mechanism in the hybrid composites.

The aim of this study is to predict the tensile strength of the hybrid fiber reinforced epoxy-polyester composites. The structural material is reinforced by $[\square/-\square]_{2S}$, $[\square/0°]_{2S}$ and $[\square/90°]_{2S}$, symmetrical laminates

made up of E-glass or carbon fibers. A particular attention was given to the examination of the damage modes of each component layer will be also determined when a ply crack was formed.

2.THEORY

The theory of the composite plates is different from that of a traditional material because of existence of coupling between bending and extension. The process of identification of elastic constants of material is based by the development of an homogenization method based on the law of mixtures [8-11]:

$$E_1 = E_f V_f + E_m(1 - V_f) \quad (1)$$

The prediction of the elastic characteristics of composite materials is done starting from the knowledge of the properties of the basic components: Ef values modulates fibers and Em modulates matrix. V_f is the voluminal fraction of fibers (Figure 1).

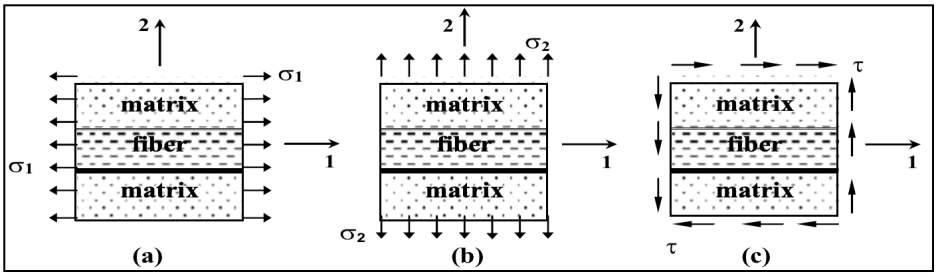

Figure 1. Various states of simple loading of a composite material:
(a) longitudinal tensile, (b) transversal tensile, (c) longitudinal Shearing.

According to the Kirchhoff hypothesis for plates [8,12], the laminate is presumed to consist of perfectly bonded laminae. The bonds are presumed to be infinitesimally thin as well non-shear-deformable. Moreover, the displacements are continuous across lamina boundaries so that no lamina can slip relative to another. The Hooke law permit to calculate the membrane efforts in function of the extensional stiffnesses Aij and the total in-plane strains $\square^0$ of the laminate:

$$[N]_{x,y} = [A]\{\square^0\}_{x,y} \quad (2)$$

The prediction of limiting strengths is determinated by Tsai-Hill criterion. It depends of strain modes related to the distortion energy; and maximum longitudinal and transversal tensile stresses (X and Y) of the [0°] ply and the maximum shear stress (S) in 1-2 plane [13,14] :

$$\left(\frac{\sigma 1}{X}\right)^{\sim} + \left(\frac{\sigma 2}{Y}\right)^{\sim} - \frac{\sigma 1 \sigma 2}{X^2} + \left(\frac{c12}{S}\right)^{\sim} \leq 1 \quad (3)$$

There is therefore no rupture of the material as long as the stresses prevailing in the latter do not exceed the ultimate stresses.

The prediction of the different failure modes and damage zones of this least resistant ply is determined by the theory of maximum stress [9,14]:

$$\sigma_1 < X \quad , \quad \sigma_2 < Y \quad , \quad r_{12} < S \quad (4)$$

If one of the inequalities is not verified, the limit state is reached, the failure then being attributed to the stress corresponding to this inequality.

2.RESULTS AND DISCUSSION

The considered composite materials are reinforced with 60% of unidirectional E-glass or carbon fibers. Reinforced resins are combinations of epoxy and polyester forming hybrid materials. Epoxy matrix layers are placed in the exterior and polyester matrix layers in the interior. The four layers constituting the laminates are alternated between +θ/-θ, +□/0° and +□/90°, symmetrically disposed about the middle surface (Figure 2).

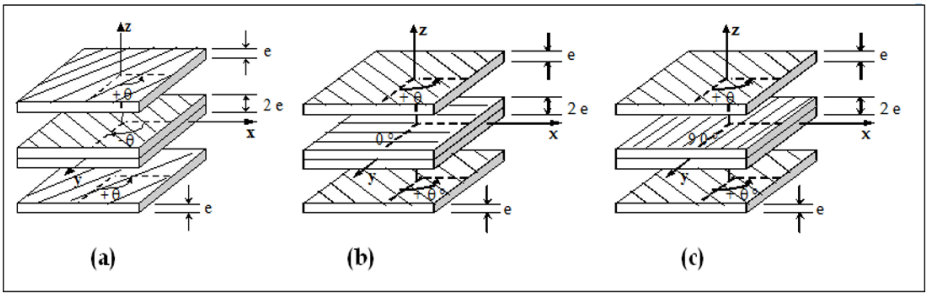

Figure 2. Definition of axis systems for symmetrical laminate: (a) [□/-□], (b) [□/0] and (c) [□/90]

Elastic constants of the basic components are illustrated in table 1. The ultimate mechanical properties of the considered composite plies are presented in table 2.

Table 1. Elastic constants of the basic components

	E1 (Gpa)	E2 (Gpa)	G12 (Gpa)	□1 2
E-Glass fiber	74	74	29.9	0.25
Carbon fiber	230	15	50	0.3
Epoxy resin	4.5	4.5	1.6	0.4
Polyster resin	4.0	4.0	1.4	0.4

Table 2. Ultimate mechanical properties of the basic composite plies

	X (Mpa)	Y (Mpa)	S (Mpa)
E-Glass/epoxy	1500	35	60
E-Glass/polyester	1500	35	60
Carbon/epoxy	1920	42	60
Carbon/polyester	1920	42	60

The behavior of the hybrid fiber reinforced epoxy-polyester composites with [□/-□]2s stacking sequence under tensile loading is represented on the Figure 3. It is noticed that the ultimate strength of the carbon/epoxy-polyester material is greater than that of E-glass/epoxy-polyester and that it gradually decreases when the fiberorientation □ varies from 0° to 90°. It is the thermosetting resin which is responsible for this degradation. These are the exterior layers which failed first either by tensile failure of the fibers (Mode I) or by shearing of the matrix parallel to the fibers (Mode III) or by traction of the mixed matrix (Mode II). It should be noted that the reinforcement with carbon fibers causes a reduction in the failure modes.

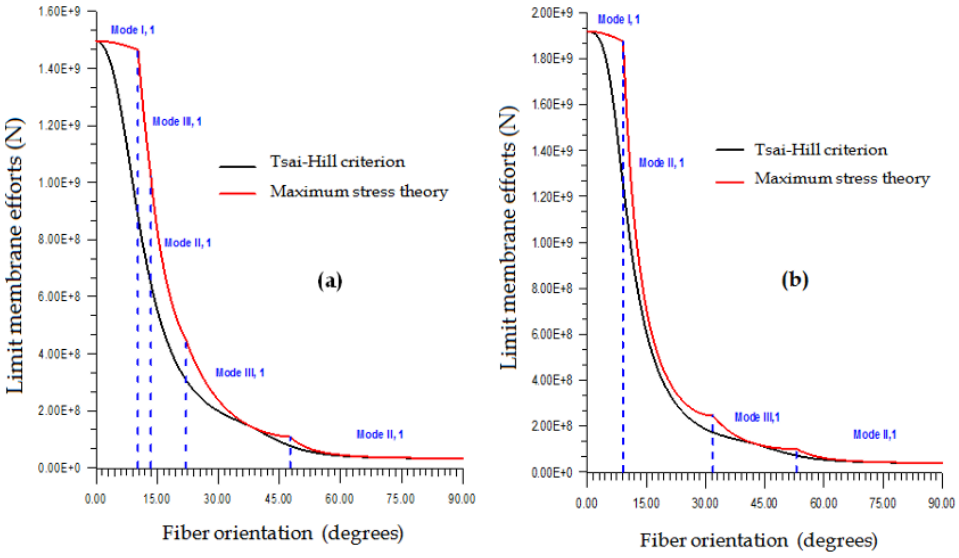

Figure 3. Variation of the limit tensile strengths of the [□/-□]2S composites reinforced with: (a) glass fibers and (b) carbon fibers

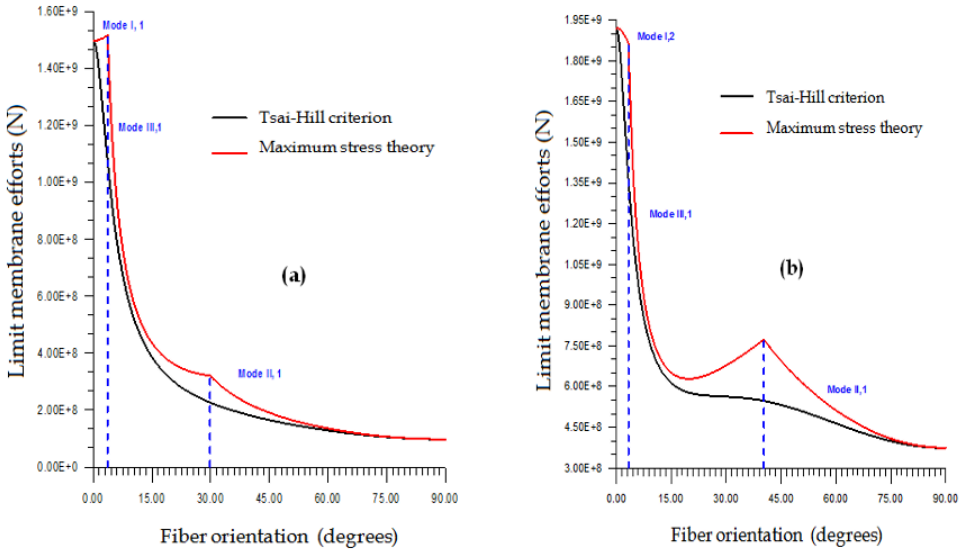

Figure 4. Variation of the limit tensile strengths of the [□/0]2S composites reinforced with: (a) glass fibers and (b) carbon fibers

Considering the [□/0]2s laminates in the figure 4, it was noticed that the hybrids become less anisotropic. These materials expose three zones of damage, the fiber tensile failure mode of which relates to the interior layer oriented at 0 °, and the other modes correspond to the exterior plies of □ orientation. The first zone is observed to be very small compared to that of balanced laminates, but the second widens when the reinforcement is provided by carbon fiber. It is the superior mechanical strength of the carbon fiber that causes the shear failure of the matrix along with the reinforcement. We also note that the resin has no influence on the resistance or the change in mechanical behavior of the material.

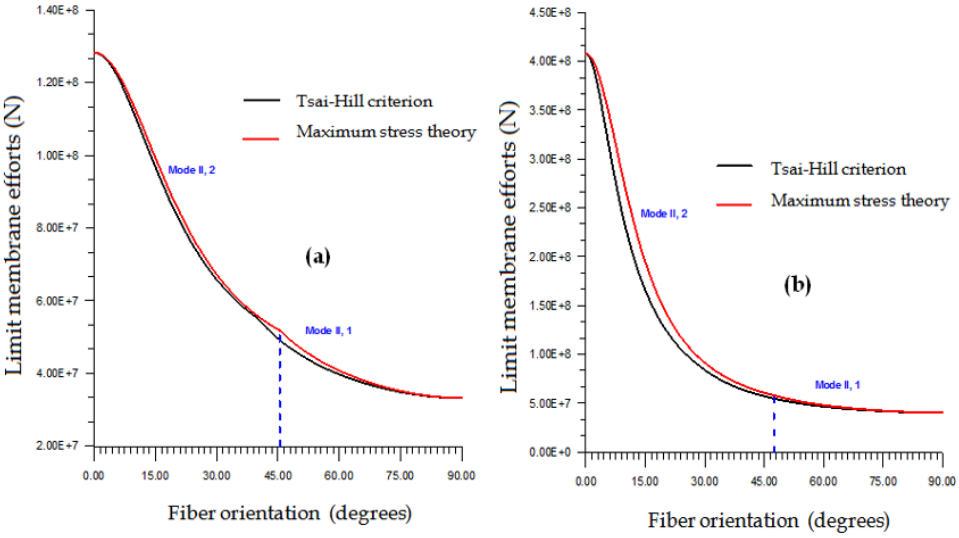

Figure 5. Variation of the limit tensile strengths of the [□/90]2S composites reinforced with: (a) glass fibers and (b) carbon fibers

In the [□/90]2S composite materials (Figure 5), there is only one failure mode by tensile of the polyester matrix constituting the interior layer of orientation 90 ° and when the orientation of the exterior plies vary from 0 ° to the vicinity of 45 °. Approaching the □= 90 °orientation, the failure will match the exterior plies with epoxy resin matrix. Reinforcement with E-glass fibers promotes rapid degradation of the strength of the hybrid composite material.

3.CONCLUSION

The study of hybrid composite materials with stacking sequence [+□/-□]2S, the mechanical strength of the laminates was not improved. On the other hand, it is noticed that the sequence [+□/0]2S presented a marked improvement in the resistance of the composite material and the profile of its mechanical behavior becomes more or less regular. Moreover, the consideration of laminated composites [□/90]2S shows an improvement in the profile of their mechanical behavior. Therefore, the presence of mixed matrices has no effect on the change in mechanical behavior. Combination of epoxy with polyester does not have a significant effect on the evaluation of the mechanical behavior of the material. Their effect only appears in the last stacking configuration but remains more or less weak. It is only noticed more considerably in the case of reinforcement of the E-glass fiber with the combination of the epoxy and polyester resins.

REFERENCES

[1] Zhang Y, Yan ZG, Ju JW, Zhu H, Chen Q. A multi-level micromechanical model for elastic properties of hybrid fiber reinforced concrete. Construction and Building Materials 2017; 152:804-817.

[2] Jing Yu, Yixin Chen, Christopher KY Leung. Micromechanical modeling of crack-bridging relations of hybrid-fiber Strain-Hardening Cementitious Composites considering interaction between different fibers. Construction and Building Materials 2018; 182:239-636.

[3] Sandeep B, Neithish Bharadwaj P, Zulfikar A, Arvind R. Development and mechanical characterizations of Kevlar/C-glass epoxy hybrid composites. Materialstoday: Proceedings 2021; 46:9092-9095.

[4] Karger-Kocsis J, Mahmood H, Pegoretti A. Recent advances in fiber/matrix interphase engineering for polymer composites. Progress in Materials Science 2015; 73 :1-43.

[5] Nalla MM, Praveen KA. Numerical and Experimental Study of the Effect of Orientation and Stacking Sequence on Petalling of Composite Cylindrical Tubes under Axial Compression. Procedia Engineering 2017; 173:1407-1414.

[6] Pandya KS, Veerraju CH, Naik NK. Hybrid composites made of carbon and glass woven fabrics under quasi- static loading. Materials & Design 2011; 32:4094-4099.

[7] Abedi MM, Nedoushan RJ, Yu WR. Enhanced compressive and energy absorption properties of braided lattice and polyurethane foam hybrid composites, International Journal of Mechanical Sciences 2021; 207:106627.

[8] Gay D. Composite materials. Hermès. Paris; 1991.

[9] Berthelot JM. Composite materials. Masson. Paris; 1996.

[10] Cussac DB, Hild F, Cabot GP. Tensile damage in concrete: Analysis of experimental technique, Journal of Engineering Mechanics 1999; 125:906-913.

[11] Stagni L. Effective transverse elastic moduli of a composite reinforced with multilayered hollow-cored fibers. Composites Science and Technology; 2001; 61:1729–1734.

[12] Kolpakov AG, Rakin SI. Homogenized strength criterion for composite reinforced with orthogonal systems of fibers. Mechanics of Materials 2020; 148:103489.

[13] Iannucci L, Ankersen J. An energy based damage model for thin laminated composites. Composites Scienceand Technology 2006; 66:934-951.

[14] Engelbrecht-Wiggans A, Leigh Phoenix S. Analysis of stress rupture data on fiber composites: Part 1- Aunified maximum likelihood method, Journal of Space Safety Engineering 2017; 4:9-14.